Quaternary Science Reviews 28 (2009) 2851–2866

Contents lists available at ScienceDirect

Quaternary Science Reviews

journal homepage: www.elsevier.com/locate/quascirev

Imprint of North-Atlantic abrupt climate changes on western European loess deposits as viewed in a dust emission model

Adriana Sima [a,b,c,*], Denis-Didier Rousseau [b,d], Masa Kageyama [a], Gilles Ramstein [a], Michael Schulz [a], Yves Balkanski [a], Pierre Antoine [e], François Dulac [a], Christine Hatté [a]

[a] Laboratoire des Sciences du Climat et de l'Environnement, UMR CEA-CNRS-UVSQ 1572, CE Saclay, l'Orme des Merisiers, Bât. 701, 91191 Gif-sur-Yvette Cedex, France
[b] Ecole Normale Supérieure, Laboratoire de Météorologie Dynamique, UMR CNRS 8539, 24 rue Lhomond, 75231 Paris Cedex, France
[c] Université Montpellier II, Institut des Sciences de l'Evolution, UMR 5554, place Eugène Bataillon, 34095 Montpellier Cedex 5, France
[d] Lamont-Doherty Earth Observatory of Columbia University, Palisades, NY 10964, USA
[e] Laboratoire de Géographie Physique, UMR CNRS 8591, CNRS, place A. Briand, 92158 Meudon, France

ARTICLE INFO

Article history:
Received 3 November 2008
Received in revised form
11 June 2009
Accepted 27 July 2009

ABSTRACT

Western European loess sequences of the last glaciation (~100,000–15,000 years BP) exhibit strong, cyclic variations of the sedimentation rate, which are coeval to the Greenland stadial/interstadial cycles and the Heinrich events. These North-Atlantic rapid climate changes appear, thus, as a potential cause for the sedimentation variations, via changes in dust intensity cycle. Here we make a first step in testing this hypothesis, by modelling the impact of the North-Atlantic abrupt climate variations on dust emission. Our dust emission calculations use meteorological fields generated by the LMDZ atmospheric general circulation model at a resolution down to 60 km over Western Europe. Three numerical experiments are run, representing a Greenland stadial, an interstadial and a Heinrich event. Orbital parameters and ice-sheet configuration correspond to conditions from Marine Isotope Stage 3 (~60,000–25,000 years BP), a period characterized by strong millennial-scale climate variability. The only differences we impose in the boundary conditions regard the North-Atlantic surface temperature and sea-ice cover in the latitudinal band 30°–63°N. The changes in wind, precipitation, soil moisture and snow cover from one simulated state to another result in small differences in dust emission intensity. In contrast, when the inhibition of the aeolian erosion by vegetation is taken into account, the dust fluxes for the cold climate states (Greenland stadial and Heinrich event) become generally more than twice higher than those for the relatively warmer Greenland interstadial, in agreement with the loess data. These results support the hypothesis that the North-Atlantic millennial-scale variability is imprinted in Western European loess profiles, and point to vegetation changes as the main factor responsible for millennial-scale sedimentation variations. An analysis for the English Channel and southern North Sea areas, major potential dust sources, shows that the seasonality of dust emission is not controlled by the wind speed, as in modern large deserts, but by the surface conditions. Consequently, the dusty season lasts from late winter to early summer, with maximum activity in April–May, and is shifted towards summer when the climate is colder.

1. Introduction

The dust cycle responds with high sensitivity to climate changes. Therefore, studying the aeolian dust deposits (loess, coversands) has greatly enriched our knowledge on the impact of past climate variations in continental domain (Kukla, 1975, 1977; Lautridou, 1985; Liu et al., 1985; Liu, 1987; Pécsi, 1987; Rousseau, 1987; Pécsi, 1990; Rousseau et al., 1990, 1998; Porter and An, 1995; Muhs et al., 1999; Muhs and Zarate, 2001). In Europe, loess covers wide areas, south of the region once occupied by the Scandinavian ice sheet at its maximum extent (Kukla, 1975, 1977; Haase et al., 2007). The thickest deposits are found along major river systems as the Seine, the Rhine, or the Danube. Such periglacial braided rivers had highly contrasted regimes, with short periods of strong discharge in the snow-melting period, when they transported huge amounts of sand and silts, and almost completely dried-out beds during the

* Corresponding author. Laboratoire des Sciences du Climat et de l'Environnement, UMR CEA-CNRS-UVSQ 1572, CE Saclay, l'Orme des Merisiers, Bât. 701, 91191 Gif-sur-Yvette Cedex, France.
E-mail address: adriana.sima@gmail.com (A. Sima).

0277-3791/$ – see front matter © 2009 Elsevier Ltd. All rights reserved.
doi:10.1016/j.quascirev.2009.07.016

rest of the year. Thus, river valleys represented important deflation areas and have mainly provided the coarse loess material for the aeolian deposits (e.g., Antoine et al., 2001; Smalley et al., 2009). The fine material has been originating not only from such local sources, but also from remote areas such as the emerged continental shelf to the west of the continent, the English Channel or the south of the North Sea (Auffret, 1980; Auffret et al., 1982; Lautridou, 1985; Antoine et al., 2003b) (Fig. 1).

Detailed loess profiles have been retrieved at several locations in the European latitudinal loess belt laying between approximately 48° and 53°N (Kukla and Lozek, 1961; Kukla, 1975, 1977; Rousseau, 1987; Rousseau et al., 1998, 2001; Antoine et al., 1999; Frechen et al., 1999, 2003; Schirmer, 2000; Antoine et al., 2001; Haesaerts et al., 2003; Gerasimenko and Rousseau, 2008). For the last glaciation (approximately between 100 and 15 kyr BP), they reveal a common, cyclic stratigraphic pattern, consisting in an alternation of loess and paleosol layers which have developed in response to rapid climate variations. Numerous periglacial level marks (ice wedges, cryoturbation and solifluxion horizons) allow an accurate correlation within the European loess domain (Kukla, 1977; Antoine et al., 2001; Haesaerts et al., 2003). The loess units, characterized by high sedimentation rates, are generally interpreted as reflecting cold, dry and windy conditions. The soil layers have developed in periods with reduced or absent dust sedimentation. They reflect a still cold, but more humid climate, which favoured a relatively better developed vegetation compared to the loess deposition periods, as evidenced especially during the Middle Pleniglacial (approximately between 55 and 30 kyr BP) (Van Vliet-Lanoë, 1987; Dorman and Sellers, 1989; Hatté et al., 1998; Antoine et al., 2001; Moine et al., 2008).

These observations have raised a first important question: did a correlation exist between the rapid environmental changes revealed by the European loess sequences and the climate variability in the neighbouring North-Atlantic area? South of 48°N, variations coeval to the Dansgaard–Oeschger (DO) events (Dansgaard et al., 1993) and Heinrich (H) events (Heinrich, 1988; Bond et al., 1992; Broecker, 1994; Bond and Lotti, 1995) have been identified in other European paleoclimate records, such as $\delta^{18}O$ in stalagmites (Genty et al., 2003), or pollen in lake, marine or terrestrial sediments (Allen et al., 1999; Combourieu-Nebout et al., 2002; Sánchez Goñi et al., 2002; Müller et al., 2003). High-resolution studies on some of the thickest deposits of Western Europe have completed the picture, showing that, indeed, at least in this part of the continent, the millennial-timescale climate changes have been intimately linked to those in the North Atlantic north of 48°N as well (Antoine et al., 2001; Rousseau et al., 2002, 2007; Haesaerts et al., 2003; Hatté and Guiot, 2005). Thus, the stratigraphic succession and the grain-size records in the most detailed profiles from the Northern France, Belgium and Germany present a striking similarity with records of $\delta^{18}O$ and dust concentration in Greenland ice (Johnsen et al., 2001). Intervals of soil development appear to correspond to the warm events registered in Greenland, which we will refer to as Greenland interstadials (GIS) (NGRIP members, 2004), and intervals of strong loess deposition, to the cold phases, hereafter referred to as Greenland stadials (GS), or to H events (Antoine et al., 2001; Rousseau et al., 2002, 2007). The dust accumulation rates in continental sediments are difficult to determine with accuracy, mainly due to dating uncertainties. However, during the North-Atlantic cold periods they were considerably higher than during the warm episodes. Estimations based on loess profiles from Nussloch, Germany, indicate significant variations of the ratio of loess versus soil accumulation rates among the different millennial-timescale cycles, with up to a 5-fold difference (Rousseau et al., 2007). The different imprints of the individual GS/GIS cycles in loess records reflect the sensitivity of the dust cycle response to changes in the general climate conditions from a cycle

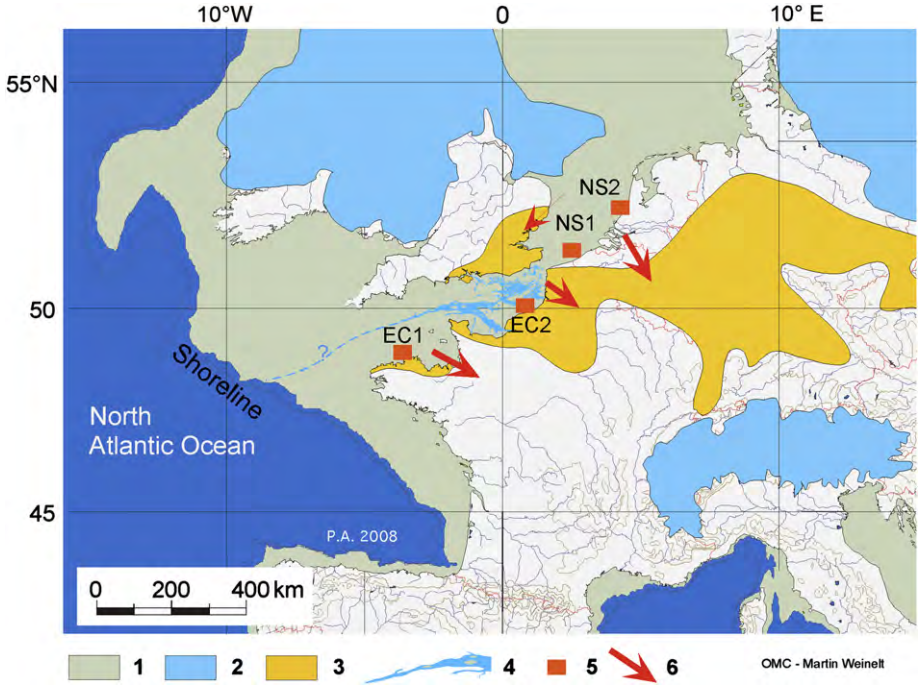

Fig. 1. Map of the studied area (modified from Antoine et al., 2003b). (1) Continental shelf, here at its maximum extent (LGM), which became exposed in glacial times due to the extension of the ice caps (2) and the consequent sea-level lowering. This has been an important dust deflation area and a source for the Western European aeolian deposits. (3) Simplified representation of the main loess area (Last Glacial). (4) Fluvial paleochannel network of the English Channel (cf. Auffret et al., 1982); the continuation to the shoreline (dashed blue line) is uncertain (Lericolais et al., 2003). (5) Grid boxes EC1, EC2, NS1 and NS2 for which dust calculations are performed (see Section 4). (6) Red arrows indicating the reconstructed main wind direction at the time of the dust deposition (cf. Lautridou et al., 1985; Antoine et al., 2003a).

to another, determined by changes in solar forcing, ice-sheet configuration, sea level, surface conditions. For each climate cycle, the sedimentation rate variations must have been due to an intensification of the dust cycle during the cold compared to the warm phases, probably via a combination of enhanced emission in the dust source areas, more efficient transport and/or deposition.

The next question is then: what are the mechanisms explaining the correlation between the North-Atlantic millennial-timescale climate changes and the loess sedimentation variations in Western Europe? Assuming that the sedimentation variations have been caused by the DO and H events is quite straightforward, but still needs to be demonstrated. Numerical modeling can be used to address this issue, by simulating the climate changes in the continental domain associated with the GS/GIS cycles and H events, and the consequent changes in the dust cycle.

A few modeling experiments have addressed the impact of the North-Atlantic millennial timescale variability on the climate in the continental domain. Those using the Earth system model of intermediate complexity (EMIC) CLIMBER-2 (e.g., Claussen et al., 2003; Jin et al., 2007) indicate a windier and drier climate in Western Europe, and thus, more favourable conditions for dust emission and transport during the North-Atlantic cold phases (GS and H events) than during the warm ones (GIS). The advantages of EMICs are that they explicitly compute the evolution of all components of the climate system (atmosphere, ocean, ice sheets, vegetation), and can perform transient experiments, but this implies the use of simplified or highly parameterized representations of some of the physical processes, and of a relatively reduced spatial resolution. Such a reduced resolution, appropriate for the purposes of the above-mentioned studies, would be too coarse for our region of interest. In contrast, the studies using atmosphere global circulation models (AGCM) benefit from more realistic physics and a higher resolution, but, as this imposes a short integration time step, they can only address selected time slices. Also, AGCMs require prescribing boundary conditions which, in the case of GIS, GS and H events, are insufficiently known. For instance, in order to investigate the response of the climate system to H events, Hostetler et al. (1999) use for their reference glacial state the CLIMAP reconstruction for the sea-surface conditions (CLIMAP project members, 1981), the modern vegetation types of Dorman and Sellers (1989), and the last glacial maximum (LGM) ice-sheet configuration from the ICE4G reconstruction (Peltier, 1994). A H event is simulated by strongly lowering the Laurentide ice sheet, and the subsequent Greenland interstadial by increasing the North-Atlantic SSTs north of 30°N to three quarters of the way from full glacial to modern values. Other AGCM studies have addressed the impact of the 14.7 kyr BP stadial–interstadial transition in the North Atlantic region (Renssen and Isarin, 2001; Renssen and Bogaart, 2003). These studies also use the CLIMAP dataset and the LGM ice-sheets for the stadial state. For the interstadial one, SSTs comparable to modern values are imposed south of 60°N, implying a considerably reduced sea-ice cover, and the LGM ice sheets are replaced by the ICE4G 14-kyr BP configuration. The land-surface conditions (vegetation cover, albedo, roughness) are adapted to the simulated stadial, respectively interstadial climates. The drastic changes of boundary conditions applied in the above AGCM studies result in important differences of atmospheric circulation in the Northern Hemisphere at temperate latitudes. Much stronger winds are simulated in the cold phases compared to the warm ones over Europe, especially in winter. Consequently, when analyzing the Late Pleniglacial wind regime in the northwest of the continent, Renssen et al. (2007) consider the "dusty season" to be autumn to spring, and the December–January–February period representative for it. This also implies the assumption of an arid environment, with negligible snow cover.

With respect to the dust cycle, as the LGM boundary conditions are relatively well known, a number of modeling studies have addressed its glacial-interglacial variations (e.g., Andersen et al., 1998; Mahowald et al., 1999; Reader et al., 1999; Werner et al., 2002). They have led to recognizing the importance of vegetation changes, along with those of atmospheric circulation and hydrological cycle, in explaining the 2–20 times higher dust deposition rates at the LGM compared to the present day (Petit et al., 1990; Steffensen et al., 1997). But no attempt has yet been made to explicitly simulate the dust-cycle variations associated with the millennial-timescale GS/GIS transitions and H events. Besides the uncertainties related to the boundary conditions, when it comes to the impact of climate variability on Western European loess build-up, other difficulties arise. The dust sources and loess deposition areas of interest here are smaller than the main arid and semi-arid areas of the world, on which most of the dust modeling experiments focus, and the European topography induces important climate differences from one location to another. Therefore, a relatively high spatial resolution is required, higher than generally achieved by the existing global paleoclimate models. Also, important deflation areas of the glacial period such as the English Channel and the southern North Sea are now submerged, and, when modeling the emission flux, hypotheses have to be made on their surface characteristics (roughness, soil texture, grain-size distribution, vegetation cover) at the time of interest.

In this work we use numerical modeling to investigate the relationship between the North-Atlantic abrupt climate changes punctuating the last glaciation and the environmental variations revealed by the Western European loess profiles. Specifically, we test if, and by which mechanisms, changes in the North-Atlantic surface conditions such as those associated with GS/GIS cycles and H events could have produced in Western Europe changes in dust emission (the initial driver of the dust cycle) consistent with the loess data, which indicate a considerably intensified dust cycle during the cold North-Atlantic phases as opposed to the warm ones. To make our simulations as realistic as possible, we employed an AGCM and a land-surface model with enhanced spatial resolution in our area of interest, and updated sea-surface conditions compared to the above studies. The models and numerical experiments are presented in Section 2. In Section 3, the simulated climate states are analyzed in terms of dust emission. Special attention is devoted to the English Channel and southern North Sea (hereafter denoted as ECSNS) area. Most of this area has been exposed between approximately 75 and 15 kyr BP, when the sea level was lower by more than 40 m than at present (Siddall et al., 2008, for a review on sea-level reconstructions) and has thus constituted a major dust source for the Western European loess deposits of the last glacial period (Juvigné, 1976; Lautridou, 1985; Antoine et al., 2003a). Our results are discussed in Section 4, and the conclusions are presented in Section 5.

2. Numerical models and experiments

We use the LMDZ.3.3 AGCM in a version with a stretched grid over Europe (Jost et al., 2005; Sepulchre et al., 2007), with a resolution down to 60 km on Western Europe. The land surface conditions are computed by the SECHIBA model (Ducoudré et al., 1993; Krinner et al., 2005), embedded in the AGCM. Three experiments are performed. The first one simulates a reference glacial state, considered to represent a Greenland stadial. The other two are designed to approximate the climatic response to changes in the North-Atlantic area such as those associated with a Greenland interstadial and an H event, respectively.

We place our experiments in an environment typical for the Marine Isotope Stage 3 (MIS3, ~60–25 kyr BP), at ~40 kyr BP,

roughly corresponding in North-Atlantic records to the sequence GS9-H4-GIS8. The H event 4 (approximately 39 kyr BP) (Bard et al., 2004) is well documented from the climate and vegetation points of view, and has been the object of previous numerical experiments with the LMDZ AGCM (Sepulchre et al., 2007). Here we use a newer version of the model and updated sea-surface conditions, but keep the focus on this period in order to be able to compare the new and previous simulations. For our reference state, assimilated to a Greenland stadial, the orbital parameters (Berger, 1978) are set to the 39-kyr BP values, the CO_2 concentration is 209 ppmv (Petit et al., 1999), and the ice-sheet configuration is the ICE4G reconstruction for 14 kyr BP (Peltier, 1994), as in Sepulchre et al. (2007) "Before H4" experiment. We consider the 14 kyr BP ice-sheet configuration to be an analog of the situation at 39 kyr BP because the sea level is roughly the same for the two periods (approximately 60 m lower than today). AGCM simulations require a global ice-sheet configuration, and this approach was the only possible at the time of running the experiments described in Sepulchre et al. (2007). For the sea-surface temperatures (SSTs) and the sea-ice cover we employ, instead of CLIMAP, the newer GLAMAP2000 reconstruction (Sarnthein et al., 2003) (Fig. 2a). In the North Atlantic, this reconstruction is generally warmer than CLIMAP, and the sea-ice extent is considerably reduced, especially in winter.

In the other two experiments, the only forcing component we modify is the surface conditions in the North Atlantic, in the latitudinal band between 30°N and 63°N, by applying zonal all-year-long SST anomalies (Fig. 2b,c). In the "H event" simulation (hereafter denoted as HE) we lower the SSTs by 2 °C between 40° and 55°N, and by values decreasing linearly to 0° at 30°N to the south and at 63°N to the north. The choice of the 2 °C maximum anomaly is based on the reconstructions by Cortijo et al. (1997). In the "Greenland interstadial" experiment (GIS) we impose warming anomalies symmetric to the HE ones: 2 °C between 40° and 55°N, +1° between 55° and 63°N, and decreasing linearly from +2 °C to 0° between 40°N and 30°N. Thus, our HE and GIS simulations are sensitivity experiments to North-Atlantic SST changes. The prescribed maximum difference of 4 °C between the HE and GIS SSTs is consistent with alkenone-based estimations from sediment cores from the central North-Atlantic (Cortijo et al., 1997). A sea-ice cover consistent with the SSTs is obtained by imposing sea ice where the SST is lower than −1.8 °C. The maximum sea-ice extent for each simulated climate state is shown in Fig. 2a–c. In each experiment the model is run for 21 years and the last 20 years are analyzed here.

The land-sea mask of the LMDZ and SECHIBA models is adapted to the ~60 m sea-level drop corresponding to the selected ice-sheet configuration. With respect to the land surface conditions, the PMIP project (Joussaume and Taylor, 1995, 2000; Harrison et al., 2002; Braconnot, 2004) recommended to use the same vegetation cover for the Last Glacial Maximum (LGM, approximately between 23 and 18 kyr BP) as for the modern or pre-industrial simulations. Here we use the same approach, except over the area of interest in this study, i.e., Western Europe. To represent the steppe-tundra environment of this area in glacial times, as suggested by palynologic evidence (e.g., de Beaulieu and Reille, 1992; Peyron et al., 1998) and other proxies (Rousseau et al., 1990; Hatté et al., 1998; Rousseau, 2001; Moine et al., 2008), we employ a combination of bare soil and two plant functional types (PFTs): C3 grass (at maximum 90% of a grid cell between 45° and 48°N, and 80% north of 48°N) and boreal evergreen needleleaf trees (up to 1%). The actual grid-cell fraction covered by each PFT is determined by the imposed maximum vegetation and the computed leaf area index (LAI). In the SECHIBA model version we use (Krinner et al., 2005), the LAI varies between minimum and maximum values fixed for each PFT to standard values based on averaged observations. The variations are only modulated by the AGCM-derived temperature: maximum and minimum LAI correspond to those of the temperature. Even though the hydrologic stress is not taken into account, the results should hold, because at middle and high latitudes the temperature is the main limiting factor in the vegetation development, not the precipitation, as is the case in the low-latitude domain (Barbour et al., 1994).

We note that some of the boundary conditions we impose are well constrained for the chosen time slice, others are "best guesses", but the processes and mechanisms we address can reasonably be assumed to operate in a wider parameter space of boundary conditions. Therefore, our results should qualitatively hold for any other Greenland stadials/interstadials and H events that have occurred during MIS3.

3. Analysis of dust emission

3.1. Key meteorological variables

The critical meteorological variables for dust entrainment, as for the entire dust cycle, are the wind speed and the precipitation (Tegen and Fung, 1994). As the emission flux depends on the wind speed cubed (Gillette, 1988; Shao and Raupach, 1993), once the erosion wind-speed threshold, which depends on the surface characteristics, is exceeded, a small increase in wind velocity induces a strong increase in the dust flux. There is also an indirect effect: strong winds help the land surface dry up rapidly after rain and become again exposed to erosion (Gillette, 1999). On the contrary, enhanced precipitation inhibits the emission. As a direct effect, it increases the soil moisture, which reinforces the soil cohesion (Fecan et al., 1999). Indirectly, on seasonal timescale, it favors the development of the vegetation, which inhibits the soil erosion by wind (e.g., Fryrear, 1985).

Besides the wind and the precipitation, at middle and high latitudes the temperature also plays an important indirect role in the dust emission variability. In the cold season, snow cover may form, which prevents aeolian soil erosion. On average, a warmer climate favors dust emission because of a reduced snow cover and a higher soil drying rate, but there is also an opposite effect: higher temperature favors vegetation development, which protects the soil from wind erosion.

The relative importance of these factors in the dust emission variations depends on the region and the time scale. Wherever snow and vegetation are present along the year, they are the main elements determining the seasonality of emissions (Tegen et al., 2002; Laurent et al., 2006). The interannual variability of the emitted dust is largely controlled by the wind speed in the major arid regions of the world at the present day (Marticorena and Bergametti, 1996; Laurent et al., 2006) as well as in glacial conditions (Werner et al., 2002), but in semi-arid regions the role of precipitation and vegetation becomes important. At glacial–interglacial time scales, the changes in the wind speed and the hydrological cycle explain only a small part of the considerably higher global dust load at the LGM compared to the present day (Joussaume, 1990; Genthon and Armengaud, 1995), as indicated by the 2–20 times higher deposition rates (Kohfeld and Harrison, 2001, and references therein). The differences of vegetation cover due to the radically different precipitation and temperature conditions have to be taken into account to improve the modeling results (Mahowald et al., 1999; Werner et al., 2002).

For a first qualitative comparison of the three simulated climate states, we examine the surface temperature, wind speed and precipitation in Western Europe (Fig. 2), especially in the latitudinal band between 48° and 53°N, which covers the ECSNS area and the

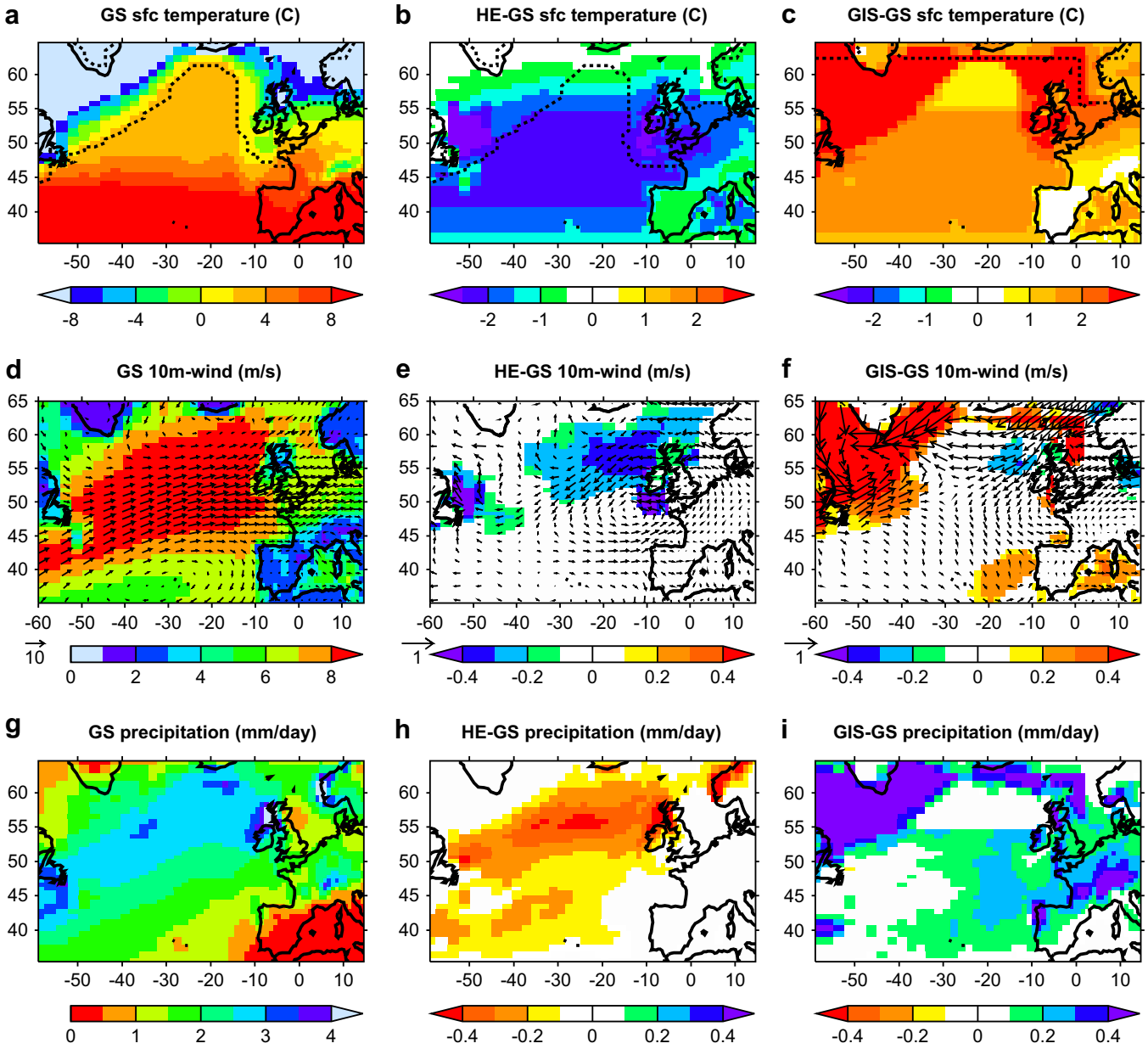

Fig. 2. Surface air temperature (a–c), 10 m-wind (d–f) and precipitation (g–i): absolute annual mean values for the reference GS state (left column) and annual mean anomalies HE–GS (middle column) and GIS–GS (right column). In white, areas where the differences are not significant at the 95% confidence level (Student's *t*-test). On the temperature maps (upper panels), the dotted lines represent the maximum (February) sea-ice extent for GS (left), HE (middle) and GIS (right). On panels (b) and (c) the zonal anomalies applied to the North-Atlantic SSTs are visible. On panel (c) temperature anomalies of more than 2.5 °C correspond to areas covered by sea ice in the GS state, but not in the GIS.

region occupied by the aeolian deposits (loess and loess derivatives; Haase et al., 2007). In the reference, GS state, the annual mean temperature is positive nearly everywhere in Western Europe (Fig. 2a), with monthly averages in the ECSNS area of up to approximately 12 °C in summer and down to −8 °C in winter (not shown). In our main area of interest the average wind speed values range between 5 and 7 m s^{-1} (Fig. 2d), with the strongest winds in winter (Fig. 5a), and the mean precipitation between 1 and 2 mm day^{-1} (Fig. 2g).

The negative anomaly applied to the North-Atlantic SSTs in the HE experiment results in a cooling on the continent, more accentuated in the northwest (up to ∼2 °C; Fig. 2b). Even though the SST anomaly applied in the adjacent North-Atlantic Ocean is constant over the year, the cooling on land is stronger in winter than in summer. For example, in the ECSNS area the monthly average of the warmest month, July, decreases by only 0.5 °C, while for the coldest month, February, the decrease is of 2.5 °C. The consequent changes in the mean wind strength and precipitation on land are very small, not significant (cf. Student's *t*-test) at the 95% confidence level (Fig. 2e,h).

For the GIS perturbation, the warming is up to ∼2 °C in the continental domain (Fig. 2c). As for HE, the temperature anomaly is strongest in the northwest, and more accentuated in winter, when the monthly mean temperatures increase by 3°–5 °C, compared to 1 °C in summer. Again, on land, the annual mean wind speed does not differ significantly from the GS climate (Fig. 2f). In the ECSNS area the monthly average differences are more important in January, March and April (Fig. 5a). The warming is accompanied by a general increase in precipitation, by 0.1–0.4 mm day^{-1} on average (Fig. 2i).

The differences between the three simulated climates with respect to wind and precipitation in annual mean, as well as in monthly means (not shown) are too small to produce changes in the dust entrainment efficiency as important as suggested by the considerable variations of the loess sedimentation rates. Analyzing these variables separately is thus not sufficient. Furthermore, Western Europe was not a completely arid area even during glacial times, but some vegetation was present, part of it changing seasonally (e.g., Woillard, 1978; Sánchez Goñi et al., 2008). Also, snow was falling not only over the Fennoscandian ice sheet, but on lower-altitude areas south of the ice sheet as well, as indicated in Western European loess profiles by niveo-aeolian (laminated) loess layers, formed especially between approximately 20 and 30 ka BP (Haesaerts et al., 1981, 2003; Lautridou, 1985; Antoine et al., 1999, 2001). The temperature differences between the millennial-timescale cold and warm episodes had an impact on the snow cover duration and extent, and on the evolution of the vegetation. Thus, to study the changes in the dust emission in Western Europe induced by millennial-timescale climate variations, we need to take into account all these factors and the way they combine along the year, which determines the dynamics of dust emissions.

3.2. Calculation of dust emission frequency and flux

The two critical factors for the dust emission are the surface conditions and the wind speed. We divide the surface conditions in two categories: (a) intrinsic characteristics, which do not change in time, as the surface roughness (vegetation excluded), the soil dry size distribution and texture of the bare soil, and (b) variable characteristics: the soil water – in solid form, as snow cover, or liquid, as top soil moisture – and the vegetation cover. The intrinsic characteristics determine the erosion threshold wind speed and the erosion potential (i.e., the maximum flux of dust available for entrainment under favourable wind speed conditions) of a surface in dry conditions and without vegetation. The variable characteristics reflect the climate influence and determine the fraction of the source area which is effectively available for dust emission at a given time.

Snow cover prevents soil erosion by wind. The soil moisture in modeling studies on the glacial dust cycle is generally accounted for by imposing a threshold moisture below which a region can be considered as a potential dust source (Joussaume, 1990; Tegen and Fung, 1994; Mahowald et al., 1999; Werner et al., 2002). However, in conditions of strong wind, the top soil layer can dry quickly and dust emission may occur even if the deeper layers are still water saturated (Gillette, 1999). Therefore, instead of soil moisture, we use a variable which better describes the surface characteristics with respect to erosion potential: the dry soil depth, also computed by the surface model. We assume that the soil must be dry on at least a 5 mm depth for a significant dust event to occur. To quantify the soil water effect we define the "dry soil fraction" fd, which combines the effects of snow and soil dryness, as follows: it equals the snow-free fraction of the source area if the soil is dry on a depth of more than 5 mm, and is 0 otherwise. We note that the SECHIBA land model does not take into account frozen ground processes, which may lead to significant underestimation/overestimation of soil temperature during soil freezing/thawing periods and underestimation of soil moisture after extensive periods of soil freezing (Koren et al., 1999). Also, soil freezing hampers dust entrainment, but this effect is included implicitly in our formulation of fd: a wet soil, frozen or not, does not allow for emission, and a dry soil, favourable to emission, cannot freeze.

Different parameterizations describe the inhibiting effect of the vegetation on wind erosion (e.g., Fryrear, 1985, and references therein). They all have in common an exponential attenuation of the erosion with increasing vegetation cover. The 2-parameter formulas of type $a\exp(-b \times fveg)$ mentioned in Fryrear (1985) have two drawbacks: they exceed the maximum possible value, 1, for vegetated soil fractions $fveg$ lower than 8–10%, and the dust emission flux never reaches zero because of the exponential dependence on $fveg$, whereas, in practice, more than 60–70% of vegetation cover suppresses the wind erosion. Alternative one-parameter formulas of type $\exp(-b \times fveg)$ (e.g., Leys, 1991) represent an improvement because they give exactly 1 for completely bare soil, but the bias for high vegetation cover remains. Here we define the vegetation factor fv (equivalent to the soil loss ratio in the above studies) using the general equation (6) of Fryrear (1985), corrected at low (<10%) and high (>60%) vegetation covers:

$$fv = \min(1, 1.81 \times \exp(-7.2 fveg)) \quad \text{if } fveg < 0.6, \text{ and } fv = 0 \text{ otherwise.}$$

In a given grid cell, a dust event occurs whenever some fraction of the area is available for dust entrainment and the wind speed exceeds the erosion threshold (w_{th}). The dust flux can be then computed as (e.g., Mahowald et al., 1999):

$$F = Cw_{10m}^2(w_{10m} - w_{th}) \quad \text{for } w_{10m} > w_{th} \ (F = 0 \text{ otherwise})$$

where C is the erosion potential, or the "source strength factor", and w_{10m} the horizontal wind velocity at 10 m above the surface.

The erosion potential C of a land surface is determined by the combination of the intrinsic characteristics and the soil water and vegetation factors defined above. We separate the two inhibiting effects by calculating first a "dry" dust flux, which only takes the soil water into account:

$$Fd = C' fd w_{10m}^2(w_{10m} - w_{th})$$

where C' depends on the intrinsic characteristics only. Introducing then the vegetation effect we obtain the actual dust flux:

$$F = fvFd = C' fdfv w_{10m}^2(w_{10m} - w_{th}) = C' E w_{10m}^2(w_{10m} - w_{th})$$

where $E = fdfv$ is the erodible fraction of soil in the grid box, both inhibiting factors being taken into account.

Erosion potentials determined for twelve major present-day arid and semi-arid regions by calibration using satellite observations vary by more than two orders of magnitude, between approximately 5×10^{-8} and 2×10^{-6} g m^{-5} s^2 (Balkanski et al., 2004). We choose for C' the intermediate value of 5×10^{-7} g m^{-5} s^2, which we keep the same in all calculations. This implies the assumption that the soil roughness (vegetation excluded), texture and grain-size distribution are the same everywhere in the studied area and for the different climates. The spatial homogeneity might be a critical choice to address absolute values of dust emission fluxes. However, here we are interested in comparing the impact of the different climates on dust emission, and we do not expect the intrinsic surface characteristics to significantly change from one state to another. Therefore, the choice of C' does not affect our results with respect to the relative dustiness of the simulated climates.

For the erosion threshold, some studies employ a single value, ranging from 0 m s^{-1} (Genthon, 1992) to 6.5 m s^{-1} (Tegen et al., 1996). Studies deriving w_{th} for the present-day deserts as a function of soil characteristics (grain-size distribution, roughness length) result in values of no less than 6 m s^{-1} (Marticorena and Bergametti, 1996; Laurent et al., 2005), comparable to the minimum wind velocities measured during dust storms in the sandy deserts of

China (Wang et al., 2003). The values of threshold velocities inferred by Balkanski et al. (2004) reach 7.5 m s^{-1} for most of the large arid and semi-arid areas. Here we assume the surface is characterized by loose material, easy to deflate, and we fix w_{th} towards the lower end of the range of realistic values, at 7 m s^{-1}. A discussion on the sensitivity of calculations to this parameter is provided in Section 3.4.

3.3. Dust emission in Western Europe

We now compare the three simulated climate states from the point of view of the surface conditions (Fig. 3). For the GS state, the annual mean dry fraction *fd* increases from northeast toward southwest (Fig. 3a). This closely reflects the distributions of the annual mean snow cover and dry soil depth, the first one decreasing, the second increasing from NE to SW, in correlation with the distributions of the mean temperature and precipitation (Fig. 2a,g).

The annual mean vegetation factor *fv* for GS is below 0.1 south of 48°N, and gradually increases northward, to about 0.5 at 54°N (Fig. 3d). It reflects the combination of the maximum vegetation cover that we imposed (cf. Section 2) and the simulated temperature. The erodible fraction $E = fdfv$ has a distribution very similar to *fv*, with average values below 1% south of 48°, and up to 6% in the southern North Sea (Fig. 3g). This result cannot be put on the expense of the stepwise change of the prescribed maximum vegetation cover, from 90% south of 48°N to 80% north of that latitude, because this feature is corrected for in the calculation of the vegetation cover, and, hence, of *fv*, by the temperature gradient. Therefore, the yearly averaged erodible fraction distribution obtained by taking into account all the involved variables is not a model artefact, but a result in agreement with the position of the dust source areas and the aeolian deposits.

The annually averaged differences of *fd*, *fv* and *E* between the reference GS state and the HE and GIS states are presented in Fig. 3, middle and right columns respectively. Relatively small differences in the average dry soil fraction are found for both the warm and the cold perturbations. Up to 10% more of a grid cell surface is dry in the GS state compared to the HE (Fig. 3b), mainly due to differences in snow cover. The GIS–GS differences only amount to up to 5% of a grid cell surface: GIS is slightly wetter than GS south of 53°N, and slightly drier to the north (Fig. 3c). This reflects the fact that the shorter snow season for GIS compared to GI is counterbalanced by enhanced precipitation (cf. Fig. 2i).

The differences are considerably larger in the case of the vegetation factor: in the latitudinal band 48°–53°N, corresponding to the ECSNS area and the main loess deposits, *fv* values for HE are higher by 0.10–0.25 than those for GS (Fig. 3e), which, in turn, are higher than the GIS values by approximately the same amount (Fig. 3f). This is explained by the fact that in our land surface model the vegetation cover is modulated by the temperature: the warmer the climate, the better the vegetation develops and, consequently, the smaller *fv* is.

The differences for the annual mean erodible fraction *E* are of generally less than 1% of a grid cell surface for HE compared to GS (Fig. 3h), and up to 3% in the favour of GS compared to GIS (Fig. 3i). The small differences reflect the fact that the soil water effect, more important in winter and for the cold states, and the vegetation inhibiting effect, predominant in summer and stronger for the warm perturbation, counterbalance in the annual average.

Such small differences with respect to the main variables relevant for dust emission, wind speed and erodible fraction, taken separately, do not allow for drawing any conclusion about the dustiness of one simulated climate state relative to another. However, dust emission is not a linear process with respect to the involved variables, and these variables change at timescales considerably smaller than a year. Therefore, our next step is to analyze how the wind and the surface conditions combine in every place at a timescale of few hours only, close to that of dust events. Thus, we use the 6-hourly model outputs to calculate the dust emission fluxes over North-Western Europe for the three simulated climate states, without the vegetation effect (*Fd*), and with vegetation effect (*F*). Fig. 4 presents the GS values (left) and the percentage ratios HE/GS (middle) and GIS/GS (right) for both *Fd* (a–c) and *F* (d–f).

For GS, the dry fraction *fd* in the North Sea is lower than in the English Channel (Fig. 3a), but the dry flux *Fd* is highest (Fig. 4a), its spatial distribution closely reflecting that of the wind speed. For the cold perturbation, *Fd* is up to approximately 130% of the GS values south of 50°N, including the southern part of the English Channel, and represents 50–100% of the GS values in the rest of the ECSNS and in the loess deposit area (Fig. 4b). The average wind speed does not significantly change between HE and GS (Fig. 2e), so that the spatial distribution of the HE/GS flux ratio is mainly determined by the differences in the dry soil fraction *fd* (Fig. 3b). The situation is similar for the warm perturbation: the average wind does not change significantly (Fig. 2f), so it has not much impact on the *Fd* distribution (Fig. 4c), which resembles that of *fd* (Fig. 3c). Thus, the GIS flux exceeds the GS one by up to 30% north of 52°N, and is generally between 70 and 100% of the GS values south of this latitude.

When taking the vegetation effect into account, in the GS state, the dustiest area is north of 48°N (Fig. 4d), coinciding with the region where the mean erodible fraction exceeds 2% (Fig. 3g). The dust flux increases from the English Channel towards the North Sea, due to a slight intensification of the wind combined with a decrease in precipitation. The area with the strongest dust flux, in the North Sea, just east of Great Britain, is also characterized by a combination of slightly stronger winds and reduced precipitation and vegetation cover compared to the rest of the region. Interestingly, in the LGM modeling study of Werner et al. (2002), the same area is predefined as a "preferential dust source" because it is a former lake bed, and appears to be only active during springtime.

The mean annual dust flux for HE is up to approximately 130% of the GS one south of 50°N, including the southern part of the English Channel, and represents 50–100% of the GS values in the rest of the ECSNS and most of the loess deposit areas (Fig. 4e). For GIS, the dust flux increases from less than 10% of the GS values in the southwest of our area of interest to approximately 80% in the northeast. It is everywhere smaller than for GS and HE (not shown) south of 53°N, and it becomes up to 40% higher than for the cold states north of that latitude (Fig. 4f). Comparing HE versus GS and GIS versus GS ratios respectively for *Fd* and $F = fvFd$, one can see that taking the vegetation into account has not much effect in the case of HE, but considerably reduces the flux for GIS with respect to the reference GS state. This fact points to the vegetation as a key factor responsible for the stadial–interstadial differences of dustiness.

3.4. Dust emission dynamics in the English Channel and the southern North Sea

To get more insight in the dust emission dynamics in the ECSNS area, we have focused on four individual grid boxes along the modern continental coast (Fig. 1). These boxes were chosen to capture the characteristics of the different parts of ECSNS region, and close to areas with thick aeolian deposits along the actual sea shore (Haase et al., 2007). Two of them, denoted as EC1 and EC2, are located south of the deep paleo-valleys of the English Channel (Auffret, 1980), at (48.93°N, 3.54°W) and (50.04°N, 0.07°W) respectively. The other two, NS1 and NS2, are in the south of the

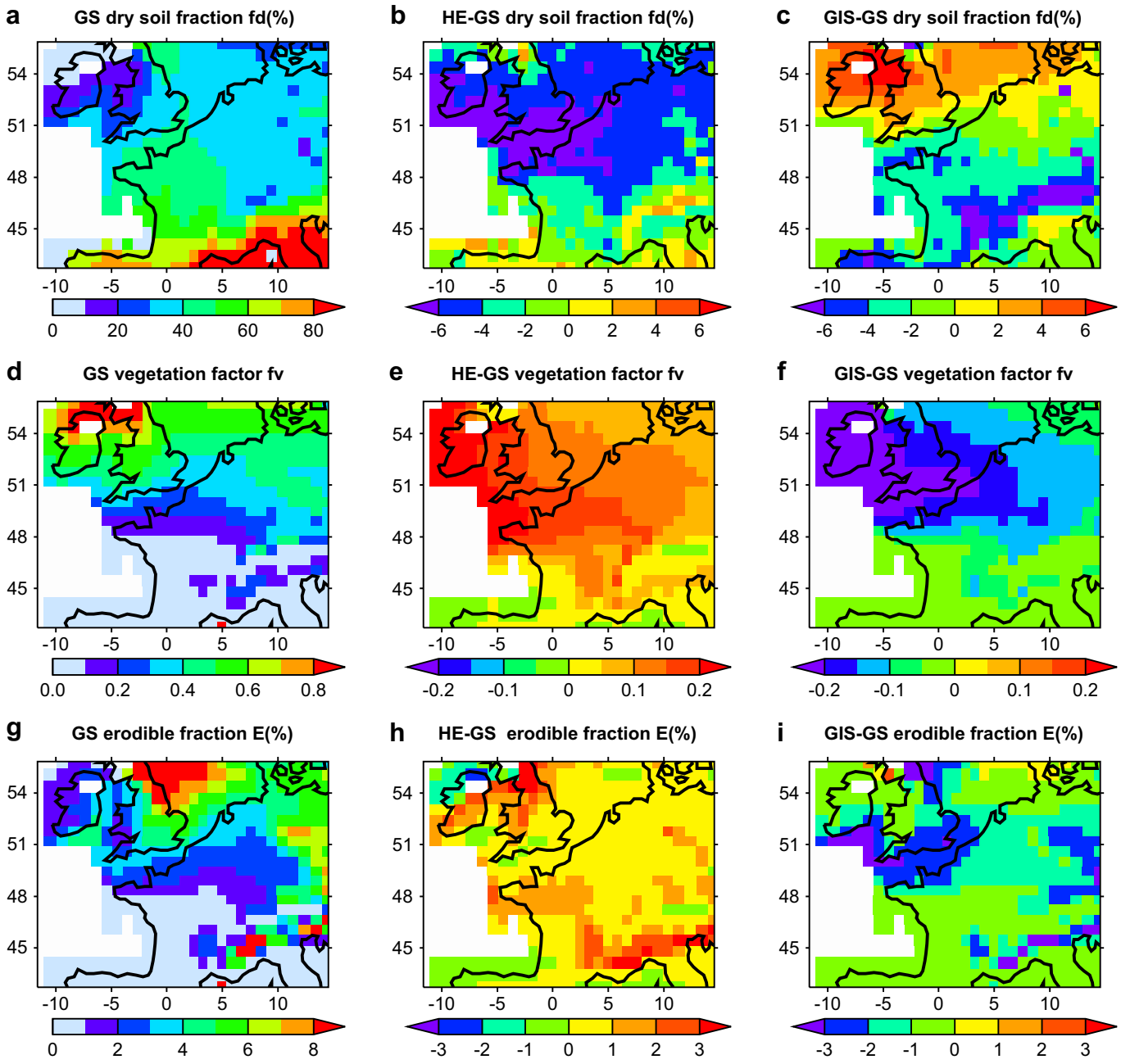

Fig. 3. Dry surface fraction *fd* (%), vegetation factor *fv* (between 0 and 1) and erodible fraction $E = fdfv$ (%): absolute values for the reference GS state (left column) and annual mean anomalies HE–GS (middle column) and GIS–GS (right column). The land-sea mask corresponds to a sea level ~60 m lower than at present. The few white grid cells on land represent fully ice-covered areas.

North Sea, centered respectively at (51.19°N, 2.43°E) and at (52.39°N, 4.1°E). The average grid cell altitude is of approximately 60 m below the sea level for EC1 (which is strongly denivelated, as the western part of the English Channel deepens abruptly away from the actual shore), 40 m for EC2, and less than 20 m for NS1 and NS2. At least the last 3 grid cells have been completely exposed during the entire typical glacial period.

We analyzed the annual cycle of wind speed and surface conditions, the influence of these variables on dust emission (event frequency and flux), and performed sensitivity experiments with respect to two key parameters, the wind threshold and the maximum vegetation cover. The calculations were based on 6-hourly data over 20 years of simulation. We have found that analyzing the four grid boxes separately provides qualitatively similar results. Therefore, in order to show a synthetic quantitative image of the ECSNS region, we present averages and other statistic calculations made for each climate state on the joined datasets for the four individual boxes.

3.4.1. Annual cycle

In all three experiments the winds are strongest in winter and spring (Fig. 5a). From December to April, even the monthly averaged wind speeds exceed our chosen erosion threshold of 7 m s^{-1}. However, precipitation is also high in these cold months, and snow cover is present, resulting in an average dry soil fraction *fd* of less than 20% (Fig. 5b). In contrast, from the end of spring until the

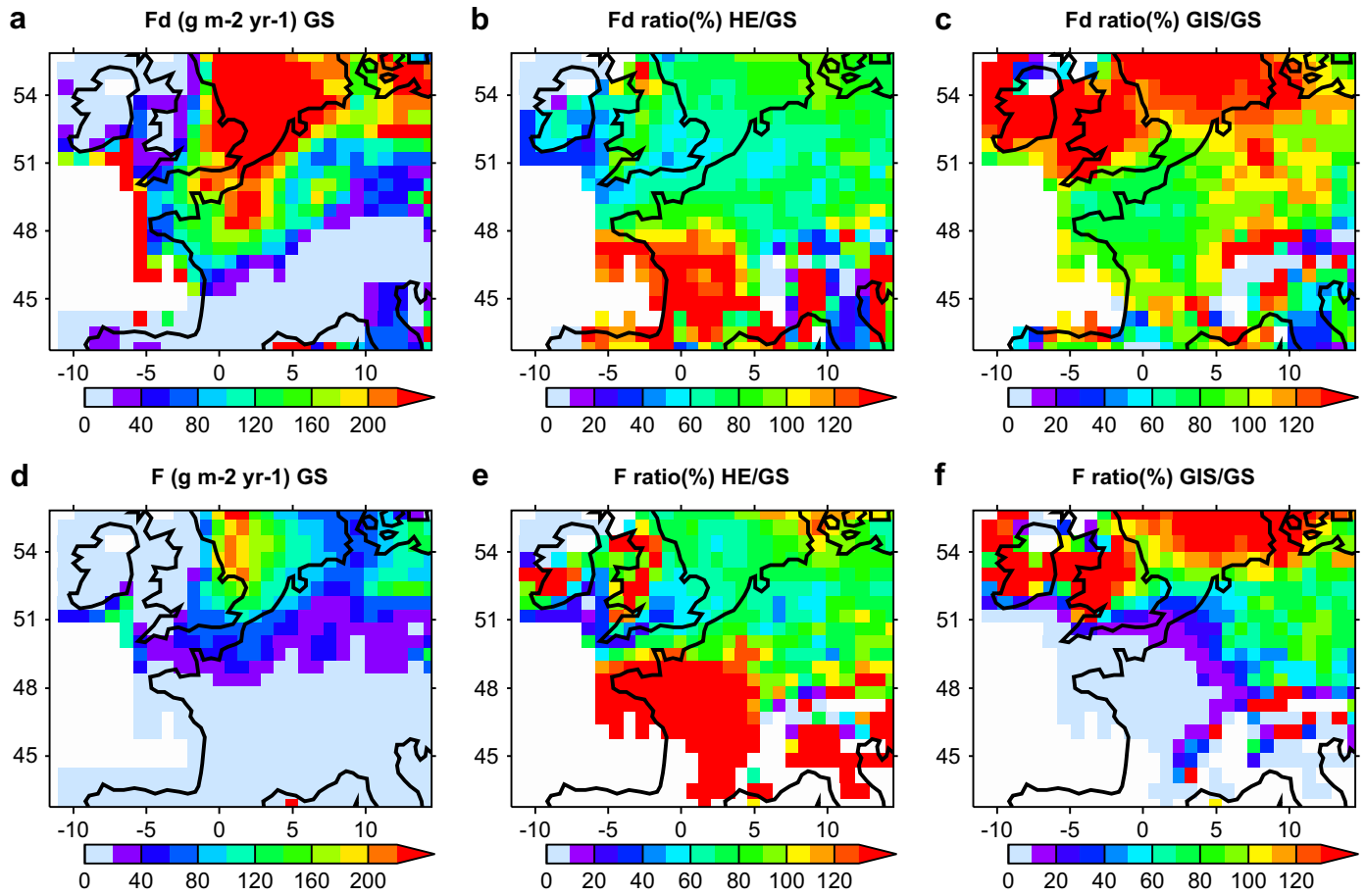

Fig. 4. Dust emission flux computed without taking the vegetation effect into account (*Fd*, upper panels), respectively with vegetation effect (*F*, lower panels): absolute values for the reference state GS (left column) and flux ratios (%) HE/GS (middle column) and GIS/GS (right column).

beginning of autumn the soil is drier (*fd* up to 85%), but the wind weakens, with a minimum of the average speed from July to September. Consequently, the dry dust flux *Fd* (Fig. 5c), calculated by only taking into account the 10 m-wind speed and the soil water, starts to increase in February-March, has a strong maximum from April to June and decreases in July and August. It shows a secondary maximum (4–5 times smaller than the one in springtime) in October, when the wind starts to intensify, and falls to zero in December and January, due to snow and soil wetness.

The vegetation factor *fv* is maximum in the cold season (when the simulated vegetation cover is reduced) and minimum in the warm one (Fig. 5b). The erodible fraction *E*, combining the soil water and vegetation factors *fd* and *fv*, is null in all experiments from July to January, which means that during this interval no dust events can occur. For GS, dust emission is active from February to May, with a maximum in April–May for both the erodible fraction *E* (15-20%) and the dust flux *F*. For GIS, the erodible fraction is generally small, with a maximum of approximately 5% in March and April. The dusty season also starts in February (when the effect of strong winds prevails over that of very restrictive surface conditions), but ends a month earlier than for GS, in April. For HE, dust events occur from March to June, with a maximum in May for both *E* (35%) and the dust flux. This shows that the usual approach of analyzing averages over the conventional seasons (e.g., December–January–February for winter) might be appropriate when the vegetation effect is not taken into account, but information would be lost when including the vegetation, because the HE dusty season is shifted by 1–2 months compared to the other two experiments.

3.4.2. Dust event frequency and dust flux

The frequency of situations when the wind exceeds the erosion threshold is almost the same for the three experiments: approximately 140 cumulated days (i.e., the number of 6-hour intervals divided by 4) per year (Fig. 6a). Quite similar values are also obtained when imposing the condition $fd > 0$ alone (Fig. 6b). As the wind is stronger in the cold part of the year, and the soil is drier in the warm one, requesting both (a) and (b) criteria to be satisfied reduces the dusty period to 20–25 days/year. Such situations occur during springtime and autumn, and their frequency, which is the frequency of dust events if the vegetation effect is not taken into account (dry dust flux $Fd > 0$), is quite similar for the three climates (Fig. 6c).

When adding the vegetation effect to that of the soil water, by imposing $fd > 0$ (condition (b)) and $fv > 0$ simultaneously, we obtain approximately 20 days/year with favourable surface conditions (i.e., $E > 0$ in at least one of the 4 grid cells) for the cold states, and only about 10 days/year in the case of the warm perturbation (Fig. 6d). Consequently, the frequency of dust events with all restrictions for surface and wind speed taken into account (conditions (a) and (d) combined) is also twice smaller for the GIS than for the GS and HE experiments, approximately 5 versus 10 days/year (in springtime and in the beginning of summer, cf. Section 4a).

Comparing the frequency of situations when $w > w_{th}$ (Fig. 6a) to that when $E > 0$ (Fig. 6d), we note that in our area of interest the dust emission is primarily limited by the surface conditions. Thus, the amount of dust entrained in the ECSNS area over a year is mainly determined by a few days of high winds in a limited period of 3–5 months when the surface conditions are favourable.

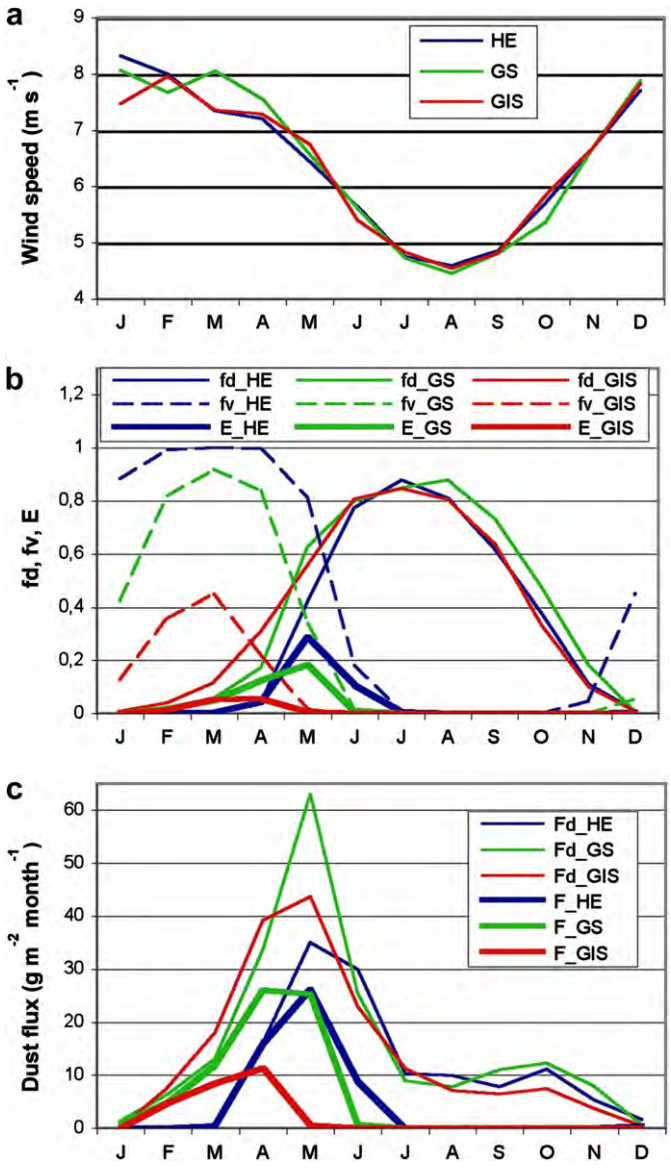

Fig. 5. The annual cycle for (a) wind speed, (b) source factors, and (c) dust flux, computed using 6-hourly data from the four selected grid boxes in the ECSNS area. The HE curves are in dark blue, the GS ones in green and the GIS ones in red. On panels (b) and (c), the dry soil fraction *fd* (representing the snow cover and soil moisture effect) and the corresponding dust flux *Fd* are in thin lines, while the erodible fraction *E* (combining soil–water and vegetation effects) and the corresponding dust flux *F* are in thick lines. The vegetation factor *fv* is represented by dashed lines on panel (b).

Fig. 7 summarizes the dust fluxes computed for each of the 20 years of simulation, using box-and-whiskers diagrams. This allows an analysis of the interannual variability of the results. Without taking the vegetation effect into account (Fig. 7a) the interannual variability is high in all three states (the flux is tripled from the 5th to the 95th percentile). GS is the dustiest, with 50% of the annual values higher than the GIS 75th percentile, whereas HE is the least dusty, with 50% of values below the GIS 25th percentile. When introducing the vegetation effect (Fig. 7b), the variability remains important, but the emission fluxes reduce considerably and the warm perturbation is clearly separated from the two cold states. GS remains the dustiest, followed by HE, with the median (50th percentile) above the GS 25th percentile, and GIS is the least dusty, with its 75th percentile below the HE median and the GS 25th percentile. Thus, even if the interannual variability is high and some annual values are higher for GIS than some of the GS and HE ones,

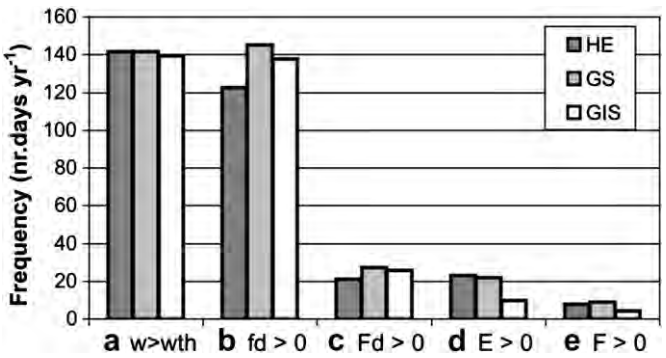

Fig. 6. The frequency, calculated from 6-hourly data from the four selected grid boxes in the ECSNS area, and expressed in number of cumulated days (i.e., number of 6-hour intervals divided by 4) per year, of the following situations: (a) the wind speed exceeds the erosion threshold w_{th} (7 m s^{-1}); (b) at least in one cell, conditions are favourable to emission from the soil water point of view only ($fd > 0$); (c) conditions (a) and (b) are simultaneously satisfied, so that a dust event would occur if vegetation is not taken into account ($Fd > 0$); (d) at least in one cell, conditions are favourable to emission from both soil-water and vegetation point of view ($E > 0$); (e) conditions (a) and (d) are simultaneously satisfied, so that a dust event occurs ($F > 0$).

the flux distribution shows that the cold climates are generally associated to stronger dust emission than the warm climate perturbation.

3.4.3. Sensitivity to the maximum vegetation cover

The maximum vegetation cover of 80% imposed north of 48°N, based on information retrieved from continental sediments (Rousseau et al., 1990; Hatté et al., 1998; Moine, 2008), is probably an overestimation for some parts of the ECSNS. Given the importance of the vegetation for the dust emission, we perform a sensitivity test by computing for each climate state the dust flux when considering at every time step only half of the simulated vegetation fraction (which implies a maximum of 40% instead of 80% of vegetation cover in each grid cell). We find that the 20-year averaged dust flux increases by approximately 100% for the GIS, 50% for the HE and 25% for the GS, but the relative order of the three climates does not change. GS remains the dustiest, HE comes in second place and GIS is the least dusty, with the flux roughly half of the GS one (Fig. 7c).

3.4.4. Sensitivity to the wind threshold

The wind threshold is another key parameter in the calculation of the dust event frequency and dust flux. Here we test whether choosing a value different from 7 m s^{-1} would change the ordering of the three climate states in terms of relative magnitude of the dust emission flux.

The wind-speed distribution over the four selected grid boxes and the 20 years of run has a similar shape in the 3 experiments for the situations when only the soil water conditions are taken into account ($fd > 0$), as well as for the situations when both soil water and vegetation criteria are satisfied, so that $E > 0$ (Fig. 8a). When only imposing the $fd > 0$ condition, the annual mean number of situations (computed from the 6-hourly model output) with the wind speed in each class in the range 2–20 m s^{-1} is higher for GS than for GIS, which, in turn, is higher than for HE. This ordering is logically found in the dust emission fluxes for the three climates (Fig. 8, lower panel). Therefore, no matter which value we choose for w_{th} within the possible interval 6–15 m s^{-1}, the relative order of the climates is the same: without considering vegetation effect (*Fd* curves on Fig. 8b), GS is the dustiest, GIS is intermediate and HE is the least dusty climate. When adding the vegetation constraint in computing dust fluxes (*F* curves), the distributions become similar for GS and HE, whereas the GIS distribution decreases to roughly

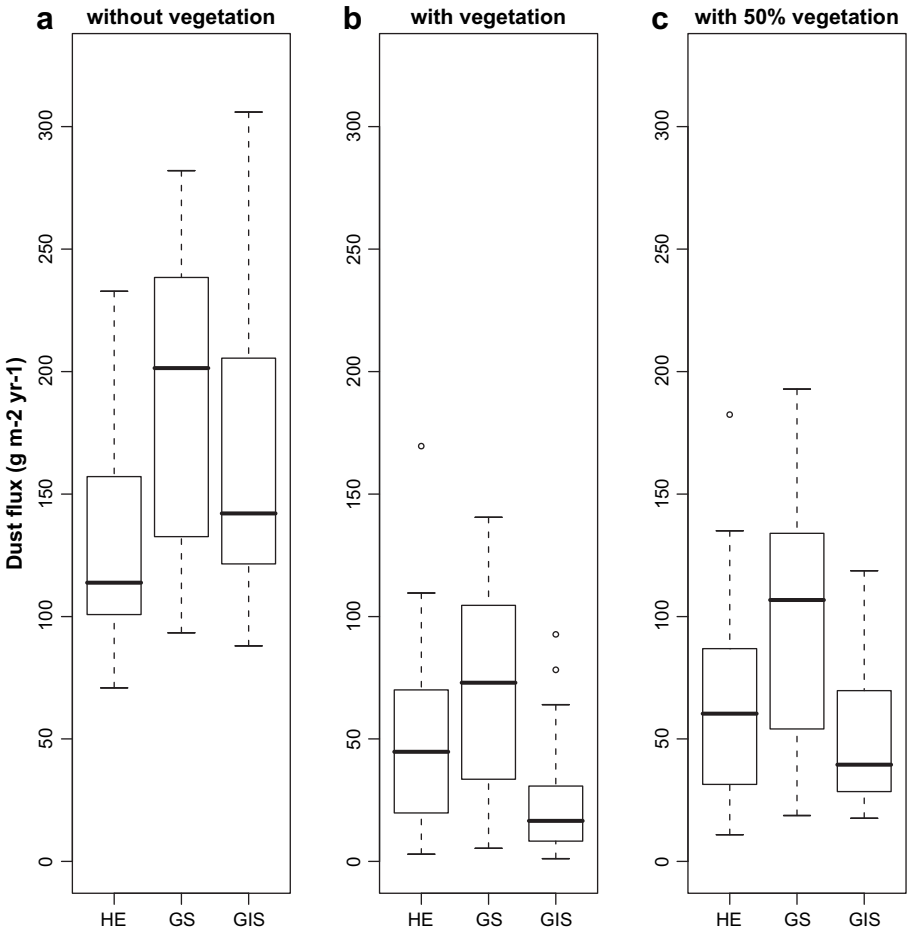

Fig. 7. Distributions of the 20 mean annual values of the GS, HE and GIS dust fluxes, computed from 6-hourly data from the four selected grid boxes in the ECSNS area. The fluxes are calculated: (a) without the vegetation effect (*Fd*), (b) with the vegetation effect (*F*), and (c) with only half of the simulated vegetation. Point (c) is meant to test the sensitivity to dust flux calculation to the vegetation cover.

half of those for the cold states. As in the case of *Fd*, whichever value we choose for w_{th} up to 15 m s^{-1}, the relative ordering of the three climates in terms of dust emission flux will always be: GS the dustiest, HE on the second place, and GS on the last one, with only approximately half of the HE flux.

We can also note that the range of wind speed values goes up to 20 m s^{-1}, but, when taking the frequency of occurrences into account for a given wind speed, the most effective wind speeds in terms of emissions are those between 9 and 14 m s^{-1}, which provide more than 70% of the annual dust flux *F*.

4. Discussion

Our simulations are, to our knowledge, the first AGCM experiments performed with a state-of-the-art model and boundary conditions, at a spatial resolution fine enough to investigate the impact of the North-Atlantic millennial-timescale variability on dust emission in Western Europe. Qualitatively, our modeling results clearly indicate that more dust is emitted in Western Europe during the North-Atlantic cold periods (Greenland stadials and H events) than during the warm episodes (Greenland, or DO interstadials). This is in accordance with the interpretation of loess data presented in the introduction, showing a considerably intensified dust cycle during the cold climate episodes compared to the warm ones. Quantitatively, the calculated frequencies and dust fluxes depend on how realistically the relevant climate variables (wind, precipitation, temperature, vegetation cover) are simulated, as well as on the accuracy of the assumptions on the erosion potential, given by intrinsic surface characteristics (texture, grain-size distribution).

A comparison of our climate modeling results to the existing EMIC studies (e.g., Claussen et al., 2003; Jin et al., 2007) is not appropriate because of the considerable difference of resolution. In our case, a relatively high spatial resolution is mandatory, considering the extent of the Western European loess deposits and of the related dust source areas, i.e., the English Channel and the south of the North Sea (ECSNS). Also, we show that understanding the factors controlling dust emission requires analyzing the high-frequency (6-hourly) model output. EMICs are not developed to simulate the atmospheric variability on such a fine timescale.

It is also difficult to compare our results with other AGCM studies as those by Hostetler et al. (1999) and Renssen et al. (2007), because they use the CLIMAP dataset for the stadial sea-surface conditions, and strongly contrasting boundary conditions for the DO- and H-type perturbations. We employ the GLAMAP2000 reconstruction, which is the most recent global reconstruction available in gridded form (Paul and Schäfer-Neth, 2003), and thus, ready to use with an AGCM. In GLAMAP2000, as well as in the newest reconstruction MARGO (Kucera et al., 2005), the sea-ice cover is considerably reduced compared to CLIMAP, especially in winter (Fig. 2a). The storm trajectories generally follow the strongest meridional temperature gradient, and in LGM simulations

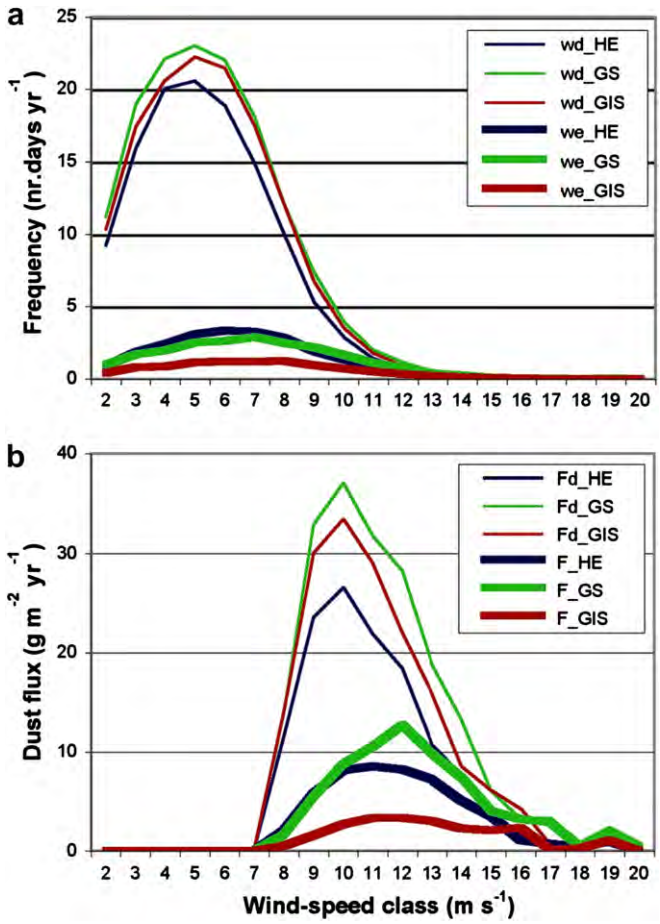

Fig. 8. (a) The wind-speed distribution, computed from 6-hourly data from the four selected grid boxes in the ECSNS area and expressed in number of cumulated days per year, for the three climates (HE in dark blue, GS in green and GIS in red), for the situations favourable to dust emission when only considering the soil-water effect ($fd > 0$ in at least one grid cell; thin lines, *wd* in the legend) and for the favourable situations from both soil-water and vegetation points of view ($E > 0$ in at least one grid cell; thick lines, *we* in the legend). (b) The dust flux as a function of wind speed: without the vegetation effect, *Fd* (thin lines), and with the vegetation effect, *F* (thick lines).

using CLIMAP surface conditions this corresponds to the ice-sheet margin (again, especially in winter, Kageyama et al., 1999). Therefore, using GLAMAP 2000 is an important update of the boundary conditions. Furthermore, the maximum difference we impose between the GIS and HE SSTs is of 4 °C, consistent with data for the central North-Atlantic (Cortijo et al., 1997). This is considerably less than the anomalies prescribed in the AGCM studies above, which are closer to the 10° to 12 °C values retrieved from cores along the European continental margin (Sánchez Goñi et al., 2008). For comparison, other reconstructed values are of 4° in the Alboran Sea (Perez-Folgado et al., 2003), and again 4° in the Western subtropical North-Atlantic (Vautravers et al., 2004). As a result, the sea-ice extent in our HE experiment does not significantly differ from the GS one, both being characterized by an ice-free central North-Atlantic even in the coldest month, February (Fig. 2a,b). Due to the latitudinal anomaly we apply, in the GSI simulation the sea ice cannot extend southward further than 63°N (Fig. 2c). The mostly ice-free North Atlantic at temperate latitudes result in simulated changes in wind and precipitation much smaller than in the other studies, and the real difference between the warm and the cold states with respect to dust emission is due to the vegetation variations. Thus, the key role of vegetation in determining glacial–interglacial changes in the dust cycle (Mahowald et al., 1999; Werner et al., 2002) appears to extend to the finer, millennial timescale. Finally, in our HE experiment the effect of lowering the ice sheets due to iceberg surging is missing, and we see our simulations as sensitivity experiments with respect to SST variations. Keeping the ice-sheet volume constant also implies no change in the extent of the deflation areas due to sea-level variations. H events could be associated with up to some tens of meters of sea-level change (Siddall et al., 2008), but this had little effect on the ECSNS area, most of which lies at less than 40 m below the actual sea level.

Our simulations indicate for the investigated period and region a significant snow cover and a high soil moisture in winter, reducing the aeolian erosion. In summer the vegetation blocking effect is at its maximum, and in autumn, the combined effect of vegetation and increasing precipitation also strongly inhibits the emission. Therefore, in contrast to the Late-Pleniglacial study of Renssen et al. (2007), we find that the dusty season is primarily determined by the surface conditions, not by wind speed, and is practically limited to late winter and springtime. More precisely, the annual dust emission flux is mainly determined in each climate state by a limited number of days with relatively strong winds (9–14 m s^{-1}) in the favourable season. We also note that in March and April the monthly average wind speed is higher in the GS than in the GIS experiment (Fig. 5a). This suggests coarser dust deposition during cold than during warm episodes, in agreement with the grain-size variations measured in the Western European loess profiles.

The model capacity of simulating strong wind events is important for quantitative estimations, and the 6-hourly data we use certainly do not reflect the entire amplitude of the daily wind cycle. However, in our qualitative comparison we may reasonably suppose that the consequences are the same for all three states, because, at least for the ECSNS key area, the wind speed annual cycle (Fig. 5a) and distribution by class (Fig. 8a) are generally similar. Thus, our results regarding the relative dustiness of the simulated climates should hold.

Precipitation is a climate parameter which is difficult to simulate with accuracy. Its over- or underestimation will affect, besides the annual dust flux, the inferred beginning of the dusty season, which is determined by the soil water inhibiting effect. For example, a reduction of the simulated precipitation would allow dust emission to start earlier, and the dust flux maximum to shift towards early springtime. The end of the dusty season would probably not be affected, because towards summer it is the vegetation effect, which takes over in determining the erodible fraction of the surface (Fig. 5b), and in our simulations the vegetation only depends on temperature. The annual dust fluxes would probably further increase in the cold states, mainly because the snow cover, already reduced in the GIS, would be diminished.

We have imposed the same composition and maximum extent of the vegetation in all three experiments, letting the differences of total vegetation cover to be only dictated by differences in temperature. Pollen studies on cores along the Iberian margin (Sánchez Goñi et al., 2008, and references therein), as well as on sediments from Jura mountains (Müller et al., 2003), show that the changes in vegetation composition due to the millennial-timescale climate variations were very important. Allowing the vegetation types to change would probably even more disadvantage the warm perturbation with respect to dust emission, as a warmer climate encourages the development of the arboreal cover, thus increasing the surface roughness and decreasing the surface wind speed.

The dust maps on Fig. 4 point to the areas most exposed to dust erosion when only taking the climate impact into account.

However, the absolute flux values presented in our figures must be considered cautiously when compared to data, because they strongly depend on the choice of the erosion potential C'. For example, in the North Sea, we obtain values up to 200 g m^{-2} yr^{-1} at 40 kyr BP, while Werner et al. (2002) find less than 10 g m^{-2} yr^{-1} at the LGM. Also, in the ECSNS area we obtain values between 20 and 140 g m^{-2} yr^{-1} at 40 kyr BP, while the mass accumulation rates at loess sites close to the ECSNS border seem to be of a few hundred g m^{-2} yr^{-1} for the Upper Pleniglacial (30–18 kyr BP) and Lateglacial (18–13 kyr BP) periods (Frechen et al., 2003, and references therein). In our dust calculations, changing the C' value would proportionally change the dust flux. Taking into account possible differences of soil characteristics from one place to another might potentially even change the spatial distribution of the most productive dust sources. The soil characteristics of the ancient ECSNS deflation area cannot be accurately reconstructed, as most of it is submerged at present, but we consider such a drastic change unlikely for the period and timescale we address.

Fig. 4 also shows that north of 53° dust emission is enhanced by up to 30% in the warm state compared to the cold ones. However, in a predominant westerly wind regime, very little dust from those latitudes could have reached the loess deposits. On the contrary, in our area of interest, ECSNS and Europe south of 53°N, GIS climate is clearly less dusty than GS and HE. How much of the entrained dust is transported towards the aeolian deposits in each of the simulated climates? In the ECSNS area, the repartition of the dust flux entrained by winds blowing from the four main sectors, SW, NW, SE and NE, shows that the proportions are generally maintained between the three simulations. Thus, for each sector the GS flux is highest, followed by the HE and then the GI Sones (Fig. 9). The most frequent "dust efficient winds" are those from the southwest sector, but in this study the interesting winds are the second most frequent ones, blowing from northwest, which are able to transport dust from the ECSNS area to the loess deposits.

Our results with respect to dust emission are qualitatively consistent with the accumulation rates in loess deposits, considerably higher during cold than during warm North-Atlantic phases (Hatté et al., 1998; Antoine et al., 2001; Rousseau et al., 2002, 2007; Hatté and Guiot, 2005; Moine et al., 2008). Certainly, although important, this is just a piece of the puzzle. Towards a meaningful comparison to loess data, the transport and the deposition processes must also be simulated. This requires a more complex model setting, including a representation of the full dust cycle.

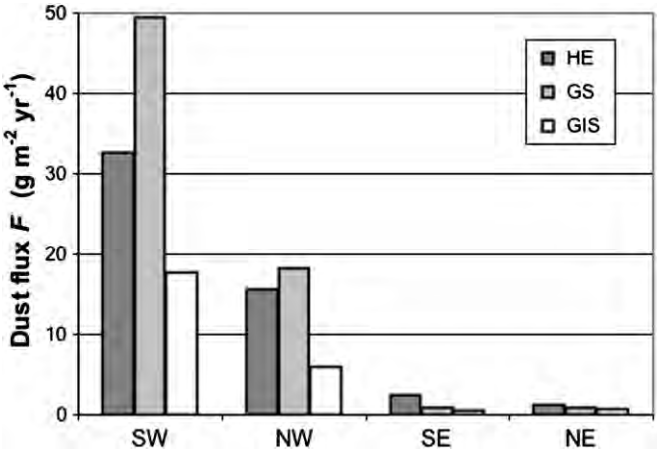

Fig. 9. The average dust flux (computed from 6-hourly data from the four selected grid boxes in the ECSNS area), entrained by winds from the main sectors: SW, NW, SE and NE for the three climate states. The important winds for this study are those from NW, which can transport dust from the ECSNS area toward the Western European aeolian deposits.

5. Conclusions and perspectives

Using numerical experiments with the LMDZ AGCM in a version with increased resolution over Western Europe, we provide a first quantification of the changes in dust emission induced in this region by the North-Atlantic abrupt climate changes punctuating the last glaciation. We find that SST changes as those associated with the North-Atlantic millennial-timescale variations result in enhanced dust emission during the cold episodes (Greenland stadials and H events) compared to the relatively warm ones (Greenland, or DO interstadials). Over most of the ECSNS area, key dust source for the Western European loess deposits, GS and HE emission fluxes are more than twice higher than the GIS fluxes. Our climate simulations also suggest that the dust transport, especially at long distance, should be more effective in the cold states, because of reduced precipitation compared to the warmer state. These first results are in agreement with the correlation established between the North-Atlantic abrupt climate changes and the variations in the loess deposition in Western Europe, based on the similarity between dust records in Greenland ice and loess profiles. Moreover, they suggest that the GS/GIS cycles and H events are the cause for these variations.

Furthermore, in order to investigate the mechanisms by which the North-Atlantic abrupt changes have caused in Western Europe the strong changes in dust emission intensity suggested by data, we evaluate the relative importance of the variations of the relevant climate components: wind, hydrological cycle, vegetation. The differences between the simulated climates with respect to wind speed are small. Precipitation is enhanced in the interstadial state, providing the soil with more water, but this is counterbalanced by evaporation, also intensified in the warmer climate. Snow covers larger areas and lasts longer in the cold states, which advantages the interstadial climate for dust emission. This effect is counteracted by vegetation, better developed in the warmer state and protecting the soil from aeolian erosion more efficiently. We conclude that vegetation control on dust emission has a crucial role in the observed millennial and sub-millennial timescale variations of the sedimentation process in the Western European loess deposits. Therefore, it should be interesting to run simulations with interactive vegetation, allowing free plant competition and taking into account both hydrologic and thermal stress. We expect this approach to result in an even stronger contrast between the cold and the warm states, because precipitation is increased for GIS compared to GS and HE, advantaging vegetation development even more than when considering only the temperature differences.

Our simulations also allow the investigation of the seasonality of dust entrainment in the different climate states. For the ECSNS area, when only taking into account the restrictions related to the soil water (snow cover and soil moisture), the dust emission is active generally from February to November, with a strong maximum in springtime and beginning of summer (April to June) and another maximum, less important, in autumn (October). When adding the restrictions related to the vegetation cover, the emission is only active from the end of winter to the beginning of summer, for 3 or 4 months in each simulated climate state. A limited number of days with high winds (9–14 m s^{-1}) in the favourable period are found to control the yearly dust emission fluxes. The HE dusty season and the period of maximum activity are shifted by 1–2 months towards summer compared to the GS and GIS states. Thus, the annual cycle of the dust emission in our area of interest appears to be controlled not by the wind cycle, as in the large arid areas, but by the surface conditions.

Here we have focused on the climate impact on the initial driver of the dust cycle: the emission. Our study indicates that model simulations of the dust emission in past climates should take into account as accurately as possible the surface characteristics in potential source areas. Furthermore, for a more quantitative model-data comparison, transport and deposition should be modelled as well, at an adequate resolution. However, we show that from the point of view of dust emission only, cold states are already dustier than interstadials. The present work is thus a first contribution to the long-term goal of simulating the complete dust cycle for the different climate states known to have occurred during the last glacial period, which will allow a comprehensive comparison with the loess data.

Acknowledgments

This study has been supported by a CNRS post-doc position for the first author and by the French CNRS/INSU through the ECLIPSE Program. The ANR-Blanc IDEGLACE is also acknowledged. The simulations have been run on the SX-6 supercomputer of the Commissariat à l'Energie Atomique. The manuscript has greatly benefited from the comments of H. Bauch and an anonymous reviewer. This is LSCE contribution 4004, LDEO contribution 7273.

References

Allen, J.R.M., Brandt, U., Brauer, A., Hubberten, H.W., Huntley, B., Keller, J., Kraml, M., Mackensen, A., Mingram, J., Negendank, J.F.W., Nowaczyk, N.R., Oberhansli, H., Watts, W.A., Wulf, S., Zolitschka, B., 1999. Rapid environmental changes in southern Europe during the last glacial period. Nature 400, 740–743.

Andersen, K.K., Armengaud, A., Genthon, C., 1998. Atmospheric dust under glacial and interglacial conditions. Geophysical Research Letters 25, 2281–2284.

Antoine, P., Rousseau, D.D., Lautridou, J.P., Hatté, C., 1999. Last interglacial–glacial climatic cycle in loess-paleosol successions of north-western France. Boreas 28, 551–563.

Antoine, P., Rousseau, D.D., Zöller, L., Lang, A., Munaut, A.V., Hatté, C., Fontugne, M., 2001. High-resolution record of the last interglacial-glacial cycle in the loess palaeosol sequences of Nussloch (Rhine Valley-Germany). Quaternary International 76/77, 211–229.

Antoine, P., Catt, J., Lautridou, J.P., Somme, J., 2003a. The loess and coversands of northern France and southern England. Journal of Quaternary Science 18, 309–318.

Antoine, P., Coutard, J.P., Gibbard, P., Hallegouet, B., Lautridou, J.P., Ozouf, J.C., 2003b. The Pleistocene rivers of the English channel region. Journal of Quaternary Science 18, 227–243.

Auffret, J.P., 1980. Les formations sédimentaires holocènes du domaine prélittoral picard. Bulletin de l'Association française pour l'Etude du Quaternaire 1–2, 34.

Auffret, J.P., Horn, R., Larsonneur, C., Curry, D., Smith, A.J., 1982. La Manche orientale, carte des paléovallées et des bancs sableux. Bureau des recherches Géologiques et Minières, Orléans.

Balkanski, Y., Schulz, M., Claquin, T., Moulin, C., Ginoux, P., 2004. The formulation of dust emissions on global scale: formulation and validation using satellite retrievals. In: Granier, C., Artaxo, P., Reeves, C. (Eds.), Emissions of Atmospheric Trace Compounds. Kluwer Academic Publishers, Dordrecht, The Netherlands, pp. 239–267.

Barbour, M.G., Burk, J.H., Pitts, W.D., 1994. Terrestrial Plant Ecology. Benjamin/Cummings Publishing Co.

Bard, E., Menot-Combes, G., Rostek, F., 2004. Present status of radiocarbon calibration and comparison records based on Polynesian corals and Iberian Margin sediments. Radiocarbon 46, 1189–1202.

Berger, A.L., 1978. Long-term variations of caloric insolation resulting from the Earth's orbital elements. Quaternary Research 9, 139–167.

Bond, G., Heinrich, H., Broecker, W., Labeyrie, L., McManus, J., Andrews, J., Huon, S., Jantschik, R., Clasen, S., Simet, C., Tedesco, K., Klas, M., Bonani, G., Ivy, S., 1992. Evidence for massive discharges of icebergs into the North Atlantic Ocean during the last glacial period. Nature 360, 245–249.

Bond, G.C., Lotti, R., 1995. Iceberg discharges into the North Atlantic on millennial time scales during the last glaciation. Science 267, 1005–1010.

Braconnot, P., 2004. Modeling the last glacial maximum and mid-holocene. Comptes Rendus Geoscience 336, 711–719.

Broecker, W.S., 1994. Massive iceberg discharges as triggers for global climate change. Nature 372, 421–424.

Claussen, M., Ganopolski, A., Brovkin, V., Gerstengarbe, F.W., Werner, P., 2003. Simulated globalscale response of the climate system to Dansgaard/Oeschger and Heinrich events. Climate Dynamics 21, 361–370.

CLIMAP project members, 1981. Seasonal Reconstructions of the Earth's Surface at the Last Glacial Maximum. The Geological Society of America Map and Chart Series.

Combourieu-Nebout, N., Turon, J.L., Zahn, R., Capotondi, L., Londeix, L., Pahnke, K., 2002. Enhanced aridity and atmospheric high-pressure stability over the western Mediterranean during the North Atlantic cold events of the past 50 k.y. Geology 30, 863–866.

Cortijo, E., Labeyrie, L., Vidal, L., Vautravers, M., Chapman, M., Duplessy, J.C., Elliot, M., Arnold, M., Turon, J.L., Auffret, G., 1997. Changes in sea surface hydrology associated with Heinrich event 4 in the North Atlantic Ocean between 40 degrees and 60 degrees N. Earth and Planetary Science Letters 146, 29–45.

Dansgaard, W., Johnsen, S.J., Clausen, H.B., Dahl-Jensen, D., Gundestrup, N.S., Hammer, C.U., Hvidberg, C.S., Steffensen, J.P., Sveinbjöprnsdottir, A.E., Jouzel, J., Bond, G., 1993. Evidence for general instability of past climate from a 250-kyr ice-core record. Nature 364, 218–220.

de Beaulieu, J.L., Reille, M., 1992. The last climatic cycle at La Grande Pile (Vosges, France) a new pollen profile. Quaternary Science Review 11, 431–438.

Dorman, J.L., Sellers, P.J., 1989. A Global Climatology of Albedo, Roughness Length and Stomatal-Resistance for Atmospheric General-Circulation Models as Represented by the Simple Biosphere Model (Sib). Journal of Applied Meteorology 28, 833–855.

Ducoudré, N.I., Laval, K., Perrier, A., 1993. Sechiba, a new set of parameterizations of the hydrologic exchanges at the land atmosphere interface within the land atmospheric general-circulation model. Journal of Climate 6, 248–273.

Fecan, F., Marticorena, B., Bergametti, G., 1999. Parametrization of the increase of the aeolian erosion threshold wind friction velocity due to soil moisture for arid and semi-arid areas. Annales Geophysicae-Atmospheres Hydrospheres and Space Sciences 17, 149–157.

Frechen, M., Zander, A., Cilek, V., Lozek, V., 1999. Loess chronology of the last interglacial/glacial cycle in Bohemia and Morevia, Czech Republic. Quaternary Science Reviews 18, 1467–1493.

Frechen, M., Oches, E.A., Kohfeld, K.E., 2003. Loess in Europe-mass accumulation rates during the Last Glacial Period. Quaternary Science Reviews 22, 1835–1857.

Fryrear, D.W., 1985. Soil cover and wind erosion. Transactions of the Asae 28, 781–784.

Genthon, C., 1992. Simulations of desert dust and sea-salt aerosols in Antarctica with a general-circulation model of the atmosphere. Tellus 44B, 371–389.

Genthon, C., Armengaud, A., 1995. Radon-222 as a comparative tracer of transport and mixing in 2 general-circulation models of the atmosphere. Journal of Geophysical Research-Atmospheres 100, 2849–2866.

Genty, D., Blamart, D., Ouahdi, R., Gilmour, M., Baker, A., Jouzel, J., Van-Exter, S., 2003. Precise dating of Dansgaard–Oeschger climate oscillations in western Europe from stalagmite data. Nature 421, 833–837.

Gerasimenko, N., Rousseau, D.D., 2008. Stratigraphy and paleoenvironments of the last Pleniglacial in the Kyiv loess region (Ukraine). Quaternaire 19 (4), 293–307.

Gillette, D.A., 1988. Threshold friction velocities for dust production for agricultural soils. Journal of Geophysical Research-Atmospheres 93, 12645–12662.

Gillette, D.A., 1999. A qualitative geophysical explanation for "hot spot" dust emitting source regions. Contributions to Atmospheric Physics. 72 (1), 67–77.

Haase, D., Fink, J., Haase, G., Ruske, R., Pécsi, M., Richter, H., Altermann, M., Jager, K.D., 2007. Loess in Europe – its spatial distribution based on a European Loess Map, scale 1: 2,500,000. Quaternary Science Reviews 26, 1301–1312.

Haesaerts, P., Juvigné, E., Kuyl, O., Mucher, H., Roebroeks, W., 1981. Compte rendu de l'excursion du 13 juin 1981, en Hesbaye et au Limbourg Neerlandais, consacrée à la chronostratigraphie des loess du Pleistocène supérieur. Annales de la Société Géologique de Belgique 104, 223–240.

Haesaerts, P., Borziak, I., Chirica, V., Damblon, F., Koulakovska, L., van der Plicht, J., 2003. The east Carpathian loess record: a reference for the middle and late pleniglacial stratigraphy in central Europe. Quaternaire 14, 163–188.

Harrison, S.P., Braconnot, P., Joussaume, S., Hewitt, C., Stouffer, R.J., 2002. Comparison of palaeoclimate simulations enhances confidence in models. Eos, Transactions American Geophysical Union 83, 447.

Hatté, C., Guiot, J., 2005. Paleoprecipitation reconstruction by inverse modeling using the isotopic signal of loess organic matter: application to the Nussloch loess sequence (Rhine Valley, Germany). Climate Dynamics 25, 315–327.

Hatté, C., Fontugne, M., Rousseau, D.D., Antoine, P., Zoller, L., Tisnerat-Laborde, N., Bentaleb, I., 1998. ^{13}C variations of loess organic matter as a record of the vegetation response to climatic changes during the Weichselian. Geology 26, 583–586.

Heinrich, H., 1988. Origin and consequences of cyclic ice rafting in the Northeast Atlantic Ocean during the past 130,000 years. Quaternary Research 29, 142–152.

Hostetler, S.W., Clark, P.U., Bartlein, P.J., Mix, A.C., Pisias, N.J., 1999. Atmospheric transmission of North Atlantic Heinrich events. Journal of Geophysical Research 104, 3947–3952.

Jin, L., Chen, F.H., Ganopolski, A., Claussen, M., 2007. Response of East Asian climate to Dansgaard/Oeschger and Heinrich events in a couple model of intermediate complexity. Journal of Atmospheric Sciences 112, D06117.

Johnsen, S.J., Dahl-Jensen, D., Gundestrup, N., Steffensen, J.P., Clausen, H.B., Miller, H., Masson-Delmotte, V., Sveinbjörnsdottir, A.E., White, J., 2001. Oxygen isotope and palaeotemperature records from six Greenland ice-core stations: Camp Century, Dye-3, GRIP, GISP2, Renland and NorthGRIP. Journal of Quaternary Science 16, 299–307.

Jost, A., Lunt, D., Kageyama, M., Abe-Ouchi, A., Peyron, O., Valdes, P.J., Ramstein, G., 2005. High-resolution simulations of the last glacial maximum climate over

Europe: a solution to discrepancies with continental palaeoclimatic reconstructions? Climate Dynamics 24, 577–590.
Joussaume, S., 1990. 3-Dimensional simulations of the atmospheric cycle of desert dust particles using a general-circulation model. Journal of Geophysical Research-Atmospheres 95, 1909–1941.
Joussaume, S., Taylor, K.E., 1995. Status of the Paleoclimate Modeling Intercomparison Project (PMIP). In: Proceedings of the First International AMIP Scientific Conference, Monterey, CA, USA, pp. 425–430.
Joussaume, S., Taylor, K.E., 2000. The paleoclimate modeling intercomparison project. In: Braconnot, P. (Ed.), Proceedings of the Third PMIP Workshop, Canada, pp. 9–24.
Juvigné, E., 1976. Contribution à la connaissance de la stratigraphie au Quaternaire par l'étude des minéraux denses transparents entre l'Eifel et le Massif Central français et plus particulièrement en Belgique. Ph.D. Thesis. University Liège.
Kageyama, M., D'Andrea, F., Ramstein, G., Valdes, P.J., Vautard, R., 1999. Weather regimes in past climate atmospheric general circulation model simulations. Climate Dynamics 15, 773–793.
Kohfeld, K.E., Harrison, S.P., 2001. DIRTMAP: the geological record of dust. Earth-Science Reviews 54, 81–114.
Koren, V., Schaake, J., Mitchell, K., Duan, Q.Y., Chen, F., Baker, J.M., 1999. A parametrization of snow pack and frozen ground intended for NCEP weather and climate models. Journal of Geophysical Research-Atmospheres 104, 19,569–19,585.
Krinner, G., Viovy, N., de Noblet-Ducoudre, N., Ogee, J., Polcher, J., Friedlingstein, P., Ciais, P., Sitch, S., Prentice, I.C., 2005. A dynamic global vegetation model for studies of the coupled atmosphere–biosphere system. Global Biogeochemical Cycles 19, 1.
Kucera, M., Rosell-Mele, A., Schneider, R., Waelbroeck, C., Weinelt, M., 2005. Multiproxy approach for the reconstruction of the glacial ocean surface (MARGO). Quaternary Science Reviews 24, 813.
Kukla, G., 1975. Loess stratigraphy of Central Europe. In: Butzer, K.W., Isaac, G.L. (Eds.), After the Australopithecines. Mouton edit., The Hague, pp. 99–188.
Kukla, G., 1977. Pleistocene land–sea correlations. 1. Europe. Earth-Science Reviews 13, 307–374.
Kukla, G., Lozek, V., 1961. Loess and related deposits. In: Survey of Czechoslovak Quaternary. Czwartozed Europy Srodkowej i Wschodniej. INQUA 6th Int. Congr. Inst. Geol. Prace, Warszawa, vol. 34, pp. 11–28.
Laurent, B., Marticorena, B., Bergametti, G., Chazette, P., Maignan, F., Schmechtig, C., 2005. Simulation of the mineral dust emission frequencies from desert areas of China and Mongolia using an aerodynamic roughness length map derived from the POLDER/ADEOS 1 surface products. Journal of Geophysical Research-Atmospheres 110. doi:10.1029/2004jd005013.
Laurent, B., Marticorena, B., Bergametti, G., Mei, F., 2006. Modeling mineral dust emissions from Chinese and Mongolian deserts. Global and Planetary Change 52, 121–141.
Lautridou, J.P., 1985. Le cycle périglaciaire Pléistocène en Europe du Nord-Ouest et plus particulièrement en Normandie. Unpublished Thèse Doctorat es Sciences thesis, Université Caen.
Lautridou, J.P., Sommé, J., Heim, J., Puisségur, J.J., Rousseau, D.D., 1985. La stratigraphie des loess et formations fluviatiles d'Achenheim (Alsace): Nouvelles données bioclimatiques et corrélations avec les séquences Pléistocènes de la France du Nord-Ouest. In: Campy, M. (Ed.), Dynamical and chronological relations between glacial and periglacial deposits. Bulletin de l'Association française pour l'étude du Quaternaire 22–23, 125–132.
Lericolais, G., Auffret, J.P., Bourillet, J.F., 2003. The Quaternary channel river: seismic stratigraphy of its palaeo-valleys and deeps. Journal of Quaternary Science 18, 3–4. 245–260.
Leys, J.F., 1991. Towards a better model of the effect of prostrate vegetation cover on wind erosion. Vegetation 91, 49–58.
Liu, T.S., 1987. Aspects of Loess Research. China Ocean Press, Beijing, pp. 447.
Liu, T.S., collaborators, 1985. Loess and the Environment. China Ocean Press, Beijing.
Mahowald, N., Kohfeld, K., Hansson, M., Balkanski, Y., Harrison, S.P., Prentice, I.C., Schulz, M., Rodhe, H., 1999. Dust sources and deposition during the last glacial maximum and current climate: a comparison of model results with paleodata from ice cores and marine sediments. Journal of Geophysical Research 104, 15895–15916.
Marticorena, B., Bergametti, G., 1996. Two-year simulations of seasonal and interannual changes of the Saharan dust emissions. Geophysical Research Letters 23, 1921–1924.
Moine, O., 2008. West-European malacofauna from loess deposits of the Weichselian Upper Pleniglacial: compilation and preliminary analysis of the database. Quaternaire 19, 11–29.
Moine, O., Rousseau, D.D., Antoine, P., 2008. The impact of Dansgaard–Oeschger cycles on the loessic environment and malacofauna of Nussloch (Germany) during the Upper Weichselian. Quaternary Research 70, 91–104.
Muhs, D.R., Aleinikoff, J.N., Stafford, T.W., Kihl, R., Been, J., Mahan, S.A., Cowherd, S., 1999. Late Quaternary loess in northeastern Colorado: Part I-Age and paleoclimatic significance. Geological Society of America Bulletin 111, 1861–1875.
Muhs, D.R., Zarate, M.A., 2001. Late Quaternary eolian records of the Americas and their significance. In: Markgraf, V. (Ed.), Interhemispheric Climate Linkages. Academic Press, San Diego, pp. 183–216.
Müller, U.C., Pross, J., Bibus, E., 2003. Vegetation response to rapid climate change in Central Europe during the past 140,000 yr based on evidence from the Füramoos pollen record. Quaternary Research 59, 235–245.
NGRIP Members, 2004. High resolution climate record of the Northern Hemisphere reaching into the last Glacial Interglacial Period. Nature 431, 147–151.
Paul, A., Schäfer-Neth, C., 2003. Modeling the water masses of the Atlantic Ocean at the Last Glacial Maximum. Paleoceanography 18, 3-1–3-26.
Pécsi, M., French, H.M., 1987. Interprétation des loess et des formations loessiques, paléosols et argiles rouges dans les recherches du loess – Symposium international du loess en Chine. In: Pécsi, M. (Ed.), Loess and periglacial phenomena. Akadémiai Kiado, Budapest, pp. 63–86.
Pécsi, M., 1990. Loess is not just the accumulation of dust. Quaternary International 7/8, 1–21.
Peltier, W.R., 1994. Ice-age paleotopography. Science 265, 195–201.
Perez-Folgado, M., Sierro, F.J., Flores, J.A., Cacho, I., Grimalt, J.O., Zahn, R., Shackleton, N., 2003. Western Mediterranean planktonic foraminifera events and millennial climatic variability during the last 70 kyr. Marine Micropaleontology 48, 49–70.
Petit, J.R., Mounier, L., Jouzel, J., Korotkevivch, Y.S., Kotlyakov, V.I., Lorius, C., 1990. Palaeoclimatological and chronological implications of the Vostok core dust record. Nature 343, 56–58.
Petit, J.R., Jouzel, J., Raynaud, D., Barkov, N.I., Barnola, J.M., Basile, I., Bender, M., Chappellaz, J., Davis, M., Delaygue, G., Delmotte, M., Kotlyakov, V.M., Legrand, M., Lipenkov, V., Lorius, C., Pépin, L., Ritz, C., Saltzman, E., Stievenard, M., 1999. Climate and atmospheric history of the past 420,000 years from the Vostok ice core, Antarctica. Nature 399, 429–436.
Peyron, O., Guiot, J., Cheddadi, R., Tarasov, P., Reille, M., De Beaulieu, J.L., Bottema, S., Andrieu, V., 1998. Climatic reconstruction in Europe for 18,000 YR B.P. from Pollen Data. Quaternary Research 49, 183–196.
Porter, S.C., An, Z.S., 1995. Correlation between climate events in the North Atlantic and China during the last glaciation. Nature 375, 305–308.
Reader, M.C., Fung, I., McFarlane, N., 1999. The mineral dust aerosol cycle during the Last Glacial Maximum. Journal of Geophysical Research-Atmospheres 104, 9381–9398.
Renssen, H., Isarin, R.F.B., 2001. The two major warming phases of the last deglaciation at ~14.7 and ~ 11.5 ka cal BP in Europe: climate reconstructions and AGCM experiments. Global and Planetary Change 30, 117–153.
Renssen, H., Bogaart, P.W., 2003. Atmospheric variability over the ~14.7 kyr BP stadial-interstadial transition in the North Atlantic region as simulated by an AGCM. Climate Dynamics 20, 301–313.
Renssen, H., Kasse, C., Vandenberghe, J., Lorenz, S.J., 2007. Weichselian Late Pleniglacial surface winds over northwest and central Europe: a model-data comparison. Journal of Quaternary Science 22, 281–293.
Rousseau, D.D., 1987. Paleoclimatology of the Achenheim Series (Middle and Upper Pleistocene, Alsace, France) – a Malacological Analysis. Palaeogeography, Palaeoclimatology, Palaeoecology 59, 293–314.
Rousseau, D.D., 2001. Loess biostratigraphy: new advances and approaches in mollusk studies. Earth-Science Reviews 54, 157–171.
Rousseau, D.D., Puisségur, J.J., Lautridou, J.P., 1990. Biogeography of the pleistocene pleniglacial malacofaunas in Europe. Stratigraphic and climatic implications. Palaeogeography, Palaeoclimatology, Palaeoecology 80, 7–23.
Rousseau, D.D., Zoller, L., Valet, J.P., 1998. Late Pleistocene climatic variations at Achenheim, France, based on a magnetic susceptibility and TL chronology of loess. Quaternary Research 49, 255–263.
Rousseau, D.D., Gerasimenko, N., Matviischina, Z., Kukla, G., 2001. Late Pleistocene environments of the Central Ukraine. Quaternary Research 56, 349–356.
Rousseau, D.D., Antoine, P., Hatté, C., Lang, A., Zoller, L., Fontugne, M., Ben Othman, D., Luck, J.M., Moine, O., Labonne, M., Bentaleb, I., Jolly, D., 2002. Abrupt millennial climatic changes from Nussloch (Germany) Upper Weichselian eolian records during the Last Glaciation. Quaternary Science Reviews 21, 1577–1582.
Rousseau, D.D., Sima, A., Antoine, P., Hatté, C., Lang, A., Zoeller, L., 2007. Link between European and North Atlantic abrupt climatic changes over the last glaciation. Geophysical Research Letters 34. doi:10.1029/2007GL031716.
Sánchez Goñi, M.F., Cacho, I., Turon, J.L., Guiot, J., Sierro, F.J., Peypouquet, J.P., Grimalt, J.O., Shackleton, N.J., 2002. Synchroneity between marine and terrestrial responses to millennial scale climatic variability during the last glacial period in the Mediterranean region. Climate Dynamics 19, 95–105.
Sánchez Goñi, M.F., Landais, A., Fletcher, W.J., Naughton, F., Desprat, S., Duprat, J., 2008. Contrasting impacts of Dansgaard–Oeschger events over a western European latitudinal transect modulated by orbital parameters. Quaternary Science Reviews 27, 1136–1151.
Sarnthein, M., Gersonde, R., Niebler, S., Pflaumann, U., Spielhagen, R., Thiede, J., Wefer, G., Weinelt, M., 2003. Overview of Glacial Atlantic Ocean Mapping (GLAMAP 2000). Paleoceanography 18, 8-1–8-6.
Schirmer, W., 2000. Rhein Loess, ice cores and deep sea cores during MIS 2-5. Zeitschrift der Deutschen Gesellschaft für Geowissenschaften 151, 309–332.
Sepulchre, P., Ramstein, G., Kageyama, M., Vanhaeren, M., Krinner, G., Sánchez Goñi, M.F., d'Errico, F., 2007. H4 abrupt event and late Neanderthal presence in Iberia. Earth and Planetary Science Letters 258, 283–292.
Shao, Y., Raupach, M.R., 1993. Effect of saltation bombardment on the entrainment of dust by wind. Journal of Geophysical Research-Atmospheres 98, 12719–12726.
Siddall, M., Rohling, E.J., Thompson, W.G., Waelbroeck, C., 2008. Marine isotope stage 3 sea level fluctuations: data synthesis and new outlook. Reviews of Geophysics 46 (4). doi:10.1029/2007RG000226.
Smalley, I., O'Hara-Dhand, K., Wint, J., Machalett, B., Zdzislaw, J., Jefferson, I., 2009. Rivers and loess: the significance of long river transportation in the complex

event-sequence approach to loess deposit formation. Quaternary International 198, 7–18. doi:10.1016/j.quaint.2008.06.009.

Steffensen, J.P., Clausen, H.B., Hammer, C.U., Legrand, M., De Angelis, M., 1997. The chemical composition of cold events within the Eemian section of the Greenland Ice Core Project ice core from Summit, Greenland. Journal of Geophysical Research 102, 26,747–26,754.

Tegen, I., Fung, I., 1994. Modeling of mineral dust in the atmosphere – sources, transport, and optical-thickness. Journal of Geophysical Research-Atmospheres 99, 22897–22914.

Tegen, I., Lacis, A., Fung, I., 1996. The influence of mineral aerosol from disturbed soils on the global radiation budget. Nature 380, 419–422.

Tegen, I., Harrison, S.P., Kohfeld, K., Prentice, I.C., Coe, M., Heimann, M., 2002. Impact of vegetation and preferential source areas on global dust aerosol: results from a model study. Journal of Geophysical Research-Atmospheres 107. doi:10.1029/2001jd000963.

Van Vliet-Lanoë, B., 1987. Le rôle de la glace de ségrégation dans les Formations superficielles de l'Europe de l'Ouest. Unpublished Doctorat es Sciences thesis, Université Paris I.

Vautravers, M.J., Shackleton, N.J., Lopez-Martinez, C., Grimalt, J.O., 2004. Gulf Stream variability during marine isotope stage 3. Paleoceanography 19. doi:10.1029/2003pa000966.

Wang, X., Ma, Y., Chen, H., Wen, G., Chen, S., Tao, Z., Chung, Y.S., 2003. The relation between sandstorms and strong winds in Xinjiang, China. Water Air Soil Pollution 3, 67–79.

Werner, M., Tegen, I., Harrison, S.P., Kohfeld, K.E., Prentice, I.C., Balkanski, Y., Rodhe, H., Roelandt, C., 2002. Seasonal and interannual variability of the mineral dust cycle under present and glacial climate conditions. Journal of Geophysical Research-Atmospheres 107. doi:10.1029/2002jd002365.

Woillard, G., 1978. Grande pile peat bog: a continuous pollen record for the last 140,000 Years. Quaternary Research 9, 1–21.